

# Five Centuries of Groundwater Elevations Provide Evidence of Shifting Climate Drivers and Human Influences on Water Resources in North Central Florida

Evan Reed Larson<sup>1</sup>, Tom Mirti<sup>2</sup>, Thomas Wilding<sup>3</sup>, and Chris A Underwood<sup>1</sup>

<sup>1</sup>University of Wisconsin-Platteville

<sup>2</sup>Suwannee River Water Management District

<sup>3</sup>Nicolet Area Technical College

December 16, 2022

## Abstract

Groundwater depletion is a concern around the world with implications for food security, ecological resilience, and human conflict. Long-term perspectives provided by tree ring-based reconstructions can improve understanding of factors driving variability in groundwater elevations, but such reconstructions are rare to date. Here, we report a set of new 546-year tree-ring chronologies developed from living and remnant longleaf pine (*Pinus palustris*) trees that, when combined with existing bald cypress (*Taxodium distichum*) tree-ring chronologies, were used to create a set of nested reconstructions of mean annual groundwater elevation for North Central Florida that together explain 63% of the variance in instrumental measurements and span 1498–2015. Split calibration confirms the skill of the reconstructions, but coefficient of efficiency metrics and significant autocorrelation in the regression residuals indicate a weakening relationship between tree growth and groundwater elevation over recent decades. Comparison to data from a nearby groundwater well suggests extraction of groundwater is likely contributing to this weakening signal. Periodicity within the reconstruction and comparison with global sea surface temperatures highlight the role of El Niño-Southern Oscillation (ENSO) in driving groundwater elevations, but the strength of this role varies substantially over time. Atlantic and Pacific sea surface temperatures modulate ENSO influences, and comparisons to multiple proxy-based reconstructions indicate an inconsistent and weaker influence of ENSO prior to the 1800s. Our results highlight the dynamic influence of ocean-atmospheric phenomena on groundwater resources in North Central Florida and build on instrumental records to better depict the long-term range of groundwater elevations.

## Hosted file

925750\_0\_supp\_10530666\_rmsvm3.docx available at <https://authorea.com/users/566851/articles/613438-five-centuries-of-groundwater-elevations-provide-evidence-of-shifting-climate-drivers-and-human-influences-on-water-resources-in-north-central-florida>

1       **Five Centuries of Groundwater Elevations Provide Evidence of Shifting Climate**  
2       **Drivers and Human Influences on Water Resources in North Central Florida**

3  
4       **Evan R. Larson<sup>1</sup>, Tom Mirti<sup>2\*</sup>, Thomas Wilding<sup>1†</sup>, and Chris A. Underwood<sup>1</sup>**

5       <sup>1</sup>Department of Environmental Sciences & Society, University of Wisconsin-Platteville

6       <sup>2</sup> Suwannee River Water Management District, Live Oak, Florida

7  
8       Corresponding author: Evan Larson (larsonev@uwplatt.edu)

9       \* Current affiliation: Retired; †Current affiliation: Nicolet Area Technical College

10  
11       **Key Points:**

- 12       • A 517-yr reconstruction of groundwater elevation indicates recent lows in North Central  
13       Florida approached megadrought conditions
- 14       • These extreme low groundwater elevations were likely caused in part by climate drivers  
15       and amplified by groundwater extraction
- 16       • Coupled oceanic-atmospheric phenomena drive variability in the persistence of  
17       groundwater elevations in North Central Florida

18 **Abstract**

19 Groundwater depletion is a concern around the world with implications for food security,  
20 ecological resilience, and human conflict. Long-term perspectives provided by tree ring-based  
21 reconstructions can improve understanding of factors driving variability in groundwater  
22 elevations, but such reconstructions are rare to date. Here, we report a set of new 546-year tree-  
23 ring chronologies developed from living and remnant longleaf pine (*Pinus palustris*) trees that,  
24 when combined with existing bald cypress (*Taxodium distichum*) tree-ring chronologies, were  
25 used to create a set of nested reconstructions of mean annual groundwater elevation for North  
26 Central Florida that together explain 63% of the variance in instrumental measurements and span  
27 1498–2015. Split calibration confirms the skill of the reconstructions, but coefficient of  
28 efficiency metrics and significant autocorrelation in the regression residuals indicate a  
29 weakening relationship between tree growth and groundwater elevation over recent decades.  
30 Comparison to data from a nearby groundwater well suggests extraction of groundwater is likely  
31 contributing to this weakening signal. Periodicity within the reconstruction and comparison with  
32 global sea surface temperatures highlight the role of El Niño-Southern Oscillation (ENSO) in  
33 driving groundwater elevations, but the strength of this role varies substantially over time.  
34 Atlantic and Pacific sea surface temperatures modulate ENSO influences, and comparisons to  
35 multiple proxy-based reconstructions indicate an inconsistent and weaker influence of ENSO  
36 prior to the 1800s. Our results highlight the dynamic influence of ocean-atmospheric phenomena  
37 on groundwater resources in North Central Florida and build on instrumental records to better  
38 depict the long-term range of groundwater elevations.

39

40

41 **Plain Language Summary**

42 Groundwater is an important source of freshwater for municipal and agricultural uses around the  
43 world. One major challenge to ensuring groundwater use is sustainable is that long-term records  
44 of its availability are scarce. This means we do not fully understand all the factors that influence  
45 groundwater availability or how groundwater resources may change in the future. One way to  
46 expand perspectives on groundwater resources is to use proxies, such as tree rings, to estimate  
47 past environmental conditions. Our team gathered tree-ring samples from old-growth longleaf  
48 pine trees in North Central Florida to develop a record of tree growth that spanned 546 years,  
49 from 1472–2018. Climate conditions that influenced tree growth at our site also influenced  
50 groundwater elevation. Based on this relationship, we reconstructed over five centuries of  
51 groundwater elevation changes. From this reconstruction, we now know that while deeper and  
52 more prolonged droughts than anything experienced during the instrumental record occurred in  
53 the past, the combined influences of climate and groundwater extraction drove recent  
54 groundwater elevations to lows comparable to some of the worst droughts in the past 500 years.  
55 As population continues to grow in Florida, residents and water managers can expect to face  
56 more extremes in groundwater elevations.

57

58

## 59 **1 Introduction**

60 Groundwater depletion is a significant concern in many regions of the world with critical  
61 implications for food security, ecological systems, and human conflict (Bierkens & Wada, 2019;  
62 Jasechko & Perrone, 2021). In the United States, declining groundwater levels documented  
63 across several broad areas raise concerns about the impacts of extraction and overexploitation on  
64 groundwater resources at regional scales (Jasechko & Perrone, 2021). For example, groundwater  
65 elevations in parts of the southeastern United States have declined over recent decades (Sutton et  
66 al., 2021), despite instrumental and tree-ring based perspectives indicating relatively wet  
67 conditions compared to recent decades and even centuries (Pederson et al., 2012). These  
68 contrasting patterns suggest that groundwater extraction for municipal and agricultural uses is  
69 outpacing recharge rates (e.g., de Graaf et al., 2019); however, in most cases instrumental  
70 records of groundwater are too short to clearly disentangle the effects of climate variability and  
71 extraction on groundwater elevations.

72

73 The longer-term perspectives enabled by proxy-based reconstructions would be immensely  
74 useful in considering changing groundwater conditions, but groundwater elevation is a  
75 challenging target to reconstruct. First, most time series of groundwater elevations are relatively  
76 short and many include numerous gaps from missing observations. This poses a challenge for  
77 robust calibration and verification (Fritts, 1976), particularly given the long-term persistence in  
78 groundwater systems relative to other aspects of climate such as precipitation (Sutton et al.,  
79 2021). Second, spatial variability in recharge mechanisms and the climate sensitivity of  
80 groundwater systems may differ from the available proxies, particularly trees whose growth is  
81 linked to atmospheric and surface conditions (Hunter et al., 2020). Third, widespread

82 groundwater extraction for agricultural and municipal purposes is altering groundwater levels  
83 around the world (Bierkens & Wada, 2019), potentially introducing trends in groundwater levels  
84 that are unrelated to atmospheric conditions that would otherwise link patterns in tree growth to  
85 changes in groundwater levels (Ferguson & St. George, 2003). Despite these challenges, the  
86 potential value of expanding perspectives on groundwater variability over multiple centuries to  
87 better understand their human and climatic drivers is immense and worth pursuing (Gholami et  
88 al., 2017), particularly where oceanic-atmospheric phenomena influence hydrologic conditions  
89 on time scales beyond the instrumental record (Gordu & Nachabe, 2021). This is the case in the  
90 southeastern United States, where growing populations are increasing demands on groundwater  
91 resources in a region where global sea surface temperatures strongly influence hydrologic  
92 conditions (Enfield et al., 2001; Schmidt et al., 2001).

93  
94 Among southeastern U.S. aquifers, the Floridian Aquifer System (FAS) covers approximately  
95 100,000 square miles and is the primary source of drinking water for millions of residents in  
96 Florida and Georgia (Miller, 1990). Well data across the FAS show increasing extraction and a  
97 decline in elevation of about 0.1–0.15 meter per year since 1950 (Barlow, 2003; Marella &  
98 Berndt, 2005). Cones of depression have formed around major cities within the FAS, such as  
99 Jacksonville, Florida, and in some cases local potentiometric gradients have reversed over  
100 instrumental records, creating the potential for encroachment of saltwater from coastal regions or  
101 from deep parts of the aquifer that contain saltwater (Miller, 1990). The installation of high-  
102 capacity wells to provide irrigation on sandy sites has also increased groundwater extraction in  
103 more rural areas (Marella & Berndt, 2005). Concerns over these groundwater impacts have been  
104 amplified by growing populations and increased demand for water. In northern Florida alone,

105 population increased by nearly 1 million residents since the early 2000s, placing considerable  
106 new demand on water resources (BEBR, 2011, 2020). With a growing population in the region  
107 and a diminishing groundwater supply, water resource managers in the Southeastern United  
108 States could benefit from the long-term perspective on water resource variability offered by  
109 dendrochronology.

110

111 Here, we report a set of new 546-year tree-ring chronologies developed from the rings of living  
112 and remnant old growth longleaf pine (*Pinus palustris*) in North Central Florida that, when  
113 combined with existing tree-ring chronologies developed from bald cypress (*Taxodium*  
114 *distichum*), enable the first annually resolved, multi-century reconstruction of groundwater  
115 elevation for the state. The resulting reconstruction extends records of groundwater by over 450  
116 years, provides a long-term perspective on shifting climate influences on groundwater elevation,  
117 and enables contextualization of recent declines in groundwater elevations for the region that are  
118 unprecedented in the historical record.

119

## 120 **2 Methods and Results**

### 121 2.1 Study area and field methods

122 Our study area is located in Goethe State Forest (GSF), a forest reserve in close proximity to  
123 three of Florida's five water management districts: the Suwannee River Water Management  
124 District (SRWMD), the St. Johns River Water Management District, and the Southwest Florida  
125 Water Management District (Figure 1a). These districts collectively encompass over 7.75 million  
126 hectares and are responsible for water supply planning for approximately 10 million people. The

127 landscape is relatively flat with low relief. Soils are sandy and extremely well drained, with  
128 subtle changes in topography creating substantial differences in plant communities. Current  
129 vegetation includes open stands of longleaf and slash pine (*Pinus elliottii*) with a saw palmetto  
130 (*Serenoa repens*) understory in upland settings, while relief of only 1–2 m results in marshes and  
131 wetlands dominated by slash pine and bald cypress (Figure 1b, 1c). The forest is managed for  
132 timber production, restoration of wire grass (*Aristida stricta*) plant communities, and red  
133 cockaded woodpecker (*Picoides borealis*) habitat. Mechanical thinning between 2000–2007 and  
134 widespread use of prescribed fire has been used to maintain an open savanna structure. During  
135 this period of intensive management, numerous old-growth longleaf pines were identified, along  
136 with an abundance of remnant stumps from logging *ca.* 1850 (Outland III, 2004).

137

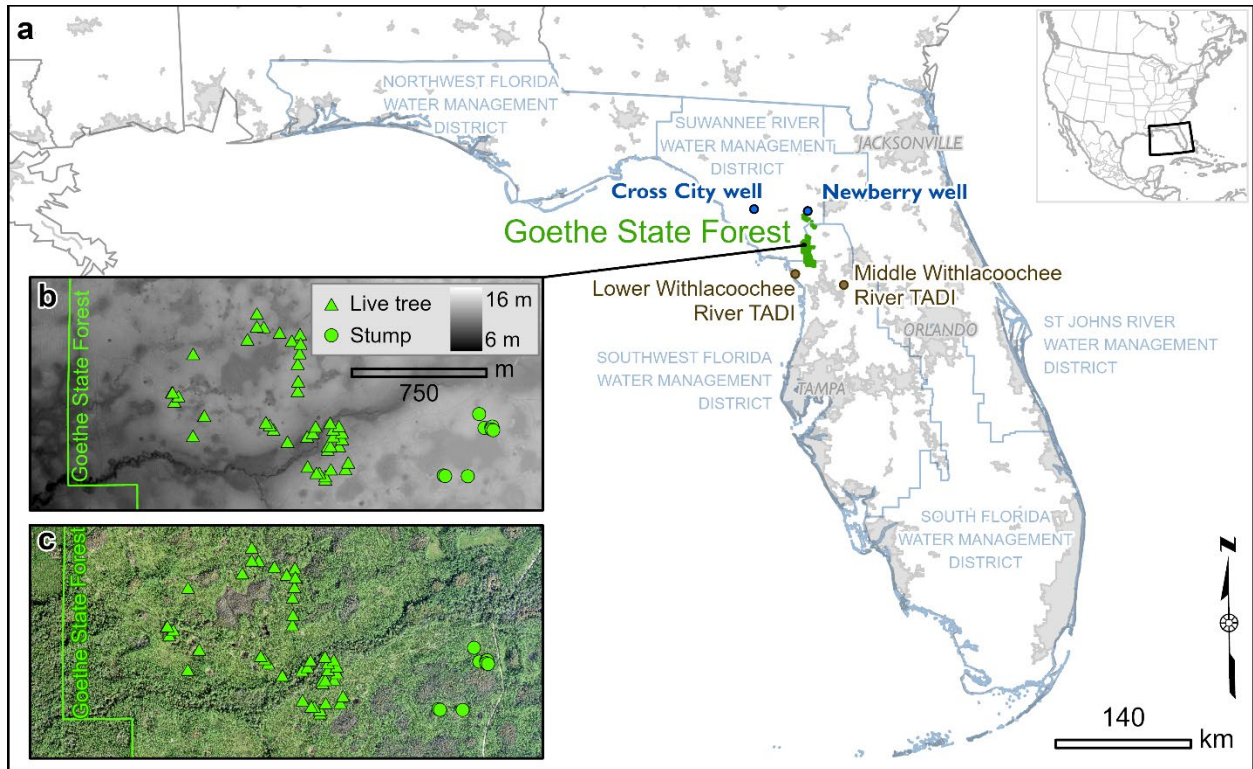
138 Groundwater elevation data are available from a network of monitoring wells that generally span  
139 the last several decades, however missing or discontinuous observations are common among  
140 these datasets. We screened numerous well logs from across the region and included two in the  
141 analyses presented here. First, the USGS Newberry well (S101722101) is the nearest long-term  
142 well to Goethe State Forest, one of the longest and most complete records investigated, and  
143 represents a continuous set of monthly observations from 1959–2020 (SRWMD, 2020). The  
144 second well considered here is the Cross City well (S101210001) which spans 1958–2020 but is  
145 more distant from the study site and includes 164 missing monthly observations, most of which  
146 occur from 1963–1979 (SRWMD, 2020). The value of the Cross City well is that it is farther  
147 from areas of intense groundwater use and should therefore represent past groundwater elevation  
148 most strongly influenced by climatic drivers rather than land use. For both wells, we calculated

149 average annual groundwater elevation from all available observations per year. The years 1974  
 150 and 1975 present gaps in the Cross City well time series where no observations were taken.

151

152

153



154

155 **Figure 1.** The study area in North Central Florida. (a) The location of Goethe State Forest  
 156 relative to the two wells used in this study, Florida water management district boundaries, and  
 157 major metropolitan areas, (b) a subset of the study area shown with a LiDAR-based DEM to  
 158 illustrate the distribution of sampled longleaf pine (*Pinus palustris*) trees and stumps relative to  
 159 subtle variations in topography, and (c) the same extent shown with color aerial imagery to  
 160 illustrate vegetation patterns created by topography.

161

162 Preliminary work in 2003 produced tree-ring chronologies from living old-growth longleaf pine  
163 and identified links between tree growth and hydrologic conditions in North Central Florida  
164 (Crockett et al., 2010). Additional sampling of both living trees and a small number of remnant  
165 stumps in 2008 produced a 438-yr chronology with significant climate information that provided  
166 important contributions to a reconstruction of the Suwannee River (Harley et al., 2017), but low  
167 sample depth in the mid-1800s coupled with a period of suppressed growth, both likely related to  
168 logging and resin extraction for the naval stores industry (Outland III, 2004), highlighted the  
169 need for additional sampling. A third phase of sampling in 2017 and 2019 specifically targeted  
170 living trees to update the existing chronologies and additional remnant longleaf pine stumps to  
171 extend the chronology further into the past, increase sample depth in the overlap between living  
172 trees and remnant stumps, and enhance signal strength during the 1800s.

173  
174 Sampling focused on living trees that visually exhibited old-growth characteristics, including the  
175 presence of robust limbs in the canopy, flattened canopy structure, absence of lower limb stubs,  
176 acute distortion of sub-canopy limbs, and the presence of peel scars associated with turpentine  
177 production, which ended around 70 years ago in northern Florida (Figure 2a, 2b). Increment core  
178 samples were collected along 1–4 radial transects of each living tree, with the number of  
179 transects determined by the shape, size, and symmetry of the tree. Stumps were initially sampled  
180 opportunistically until their value became more evident. Later, to improve the efficacy of  
181 targeted stump sampling, the study area was scouted following winter prescribed fires that  
182 reduced ground cover and maximized the likelihood of locating low-profile stumps. Stump  
183 sampling specifically targeted specimens that exhibited deep weathering, char, and evidence of  
184 box-cuts associated with resin collection activities in the 1800s. All sampled stumps were cut

185 with a chainsaw as low to the ground as possible to ensure collection of the maximum number of  
186 growth rings, with later recognition that ground-level samples also enhanced the potential for  
187 their use in fire history research (Huffman & Rother, 2017). A visual chronosequence emerged,  
188 with different types of cambial scars associated with different periods of turpentine harvesting  
189 techniques and the oldest samples coming from snags that were likely from trees that died prior  
190 to 1800s logging and turpentine activities (Figure 2b, 2c, 2d).

191



192

193 **Figure 2.** Site and tree characteristics used to guide sample collection. (a) Open stand structure  
194 has been maintained through mechanical treatments and prescribed burns, with old growth  
195 longleaf pine retained to provide habitat for the endangered red cockaded woodpecker (indicated  
196 by white band on the tree at far right). Relative sample age was estimated by (b) living trees with  
197 “catface” scars associated with turpentine activities in the late 1800s and early 1900s, (c) box  
198 cuts associated with turpentine activity in the middle to late 1800s, and (d) remnant snags with  
199 no evidence of turpentine collection from trees that likely died prior to logging or the  
200 establishment of industrial turpentine activities on site.

## 201 2.2 Tree Ring Chronology Development

202 Cross sections were frozen at *ca.*  $-20^{\circ}\text{C}$  for at least 24 hours prior to sanding to reduce the  
203 emergence of resin during the finishing process, then surfaced using hand-held belt sanders and  
204 progressing from ANSI 40-grit to ANSI 400-grit. Pneumatic palm sanders with microfinishing  
205 film were then used to maintain cool temperatures while progressively sanding to a final grit of  
206 20-micron sanding discs. Each sample was polished with steel wool to achieve the final surface.  
207 A similar progression of sanding was applied to core samples, but by hand-sanding.

208

209 Two to four paths were identified on each cross section, depending on the shape and condition of  
210 the sample, while a single transect was identified on each core sample. The annual rings of each  
211 sample were identified under  $4.5\text{--}40\times$  magnification and internally crossdated to account for  
212 locally-absent growth rings and intra-annual variations in wood density, commonly referred to as  
213 false rings. Each path was scanned at 1800 dpi optical resolution using an Epson 10000XL  
214 flatbed scanner. The images of each path were imported to WinDENDRO v2014 and measured  
215 for total ring width (TRW), earlywood width (EW), and latewood width (LW). The boundary  
216 between earlywood and latewood growth was determined as the first formation of latewood cells  
217 within each ring and a regression-based latewood measurement series ( $LW_{\text{reg}}$ ) was created for  
218 each path by removing the shared variability between earlywood and latewood widths through  
219 linear regression (*sensu* Griffin et al., 2011).

220

221 Crossdating was strong within the final longleaf pine tree-ring data set, with a total of 172 dated  
222 measurement series from 91 trees, of which 59 were living and 32 were remnants. The data set  
223 spanned the years 1472–2018 and exhibited an expressed population signal of  $>0.85$  from 1505–

224 2018 (Figure 3a, 3b). Visual inspection of the raw longleaf pine ring width data indicated a  
225 distinct decade or more of suppressed growth from the late 1800s to the early 1900s, likely the  
226 result of extensive cambial damage from turpentine activities, followed by growth releases  
227 (Figure 3a). We emphasized the variability likely related to interannual climate variations despite  
228 these releases and suppressions in tree growth by normalizing each ring-width measurement  
229 series using a power transformation method described by Cook and Peters (1997). The  
230 normalized measurement series were then used to develop a total of 16 versions of standardized  
231 ring width-index (RWI) chronologies from the longleaf pine, as described below.

232  
233 First, two versions of standard (STD) chronologies were created for each type of measurement  
234 collected from the longleaf pine (TRW, EW, LW, and  $LW_{reg}$ ). Each normalized measurement  
235 series was fit with a spline of 50% frequency cutoff at a 30-year frequency to remove low-  
236 frequency variability from the ring width series (Cook & Peters, 1981). The values from each  
237 resulting ring-width index series were then used to calculate an annually-resolved RWI  
238 chronology using a robust bi-weight mean (Cook, 1985). This resulted in chronologies with  
239 minimal evidence of the disturbance effects (GSF30; Figure 3b). Second, each normalized  
240 measurement series was fit using a stiffer spline with 50% frequency cutoff at the 100-year  
241 frequency to retain a greater proportion of the low-frequency variability within the ring-width  
242 series, and again combined into RWI chronologies using bi-weight means of annual values. The  
243 resulting chronologies retained more information that could provide insight to the low-frequency  
244 variability of hydrologic conditions in Florida, but also retained more evidence of the growth  
245 suppression (GSF100; Figure 3b). This produced eight STD chronologies, including TRW, EW,  
246 LW, and  $LW_{reg}$  based on both the GSF30 and GSF100 standardization approaches.

247  
248 Second, an additional eight residual (RES) chronologies were created by applying the same  
249 standardization methods described above (GSF30 and GSF100), but fitting each of the individual  
250 ring width index series to an Autoregressive-Moving-Average Model before combining the  
251 resulting annual values using a robust bi-weight mean (Meko, 1981). The RES chronologies  
252 therefore expressed less autocorrelation and better emphasized inter-annual variations of tree  
253 growth than the STD chronologies. In all, this resulted in a total of sixteen standardized tree-ring  
254 chronologies from the longleaf pine measurements: standard (STD) and residual (RES)  
255 chronologies based on TRW, EW, LW, and  $LW_{reg}$ , with two versions of each chronology based  
256 on standardization with 30-year smoothing splines (GSF30) and 100-year smoothing splines  
257 described above (GSF100).

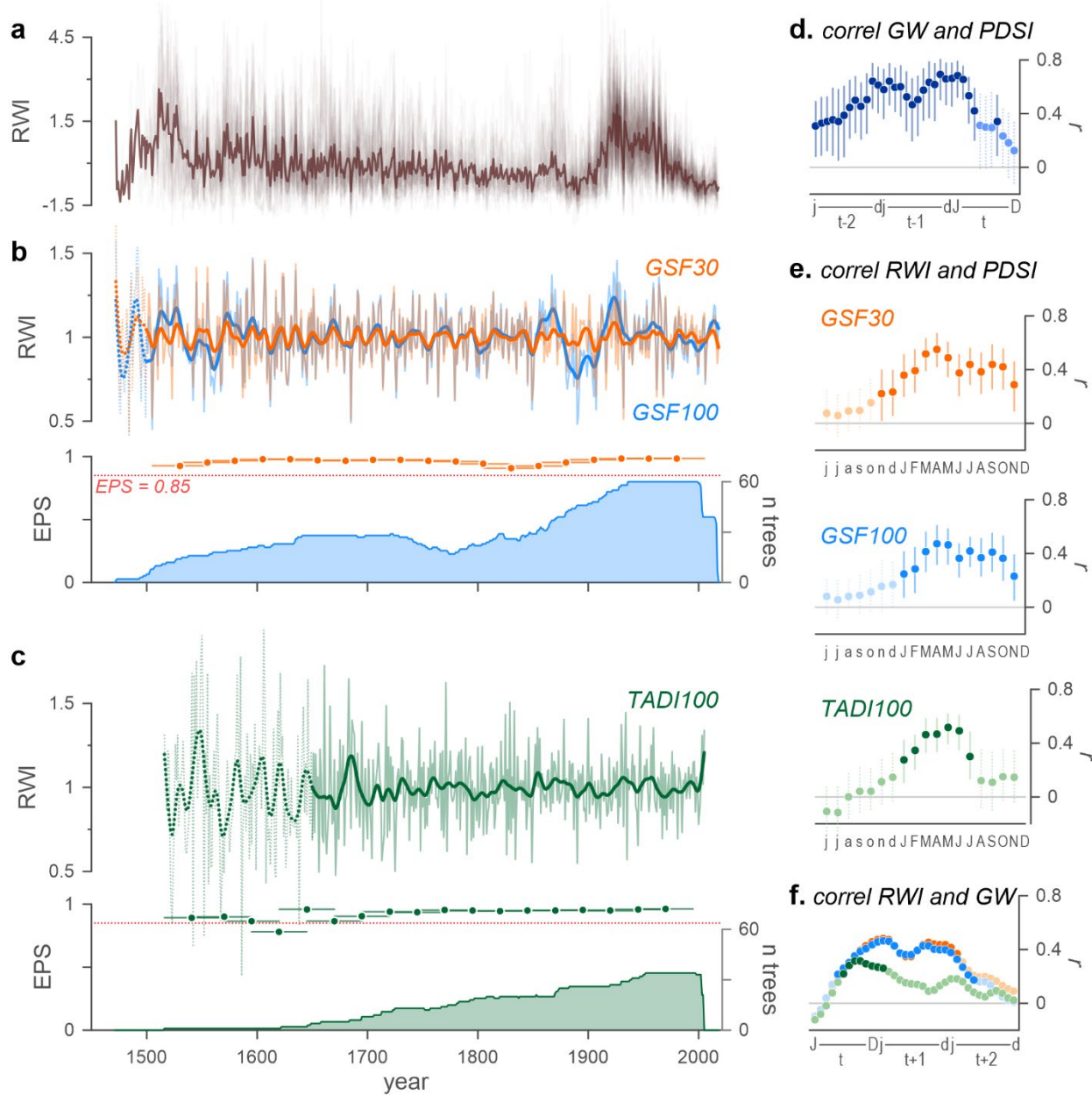
258  
259 In addition to the newly developed longleaf pine chronologies, tree-ring width data from  
260 previously developed bald cypress trees (*Taxodium distichum*) growing at two nearby sites along  
261 the Withlacoochee River were collected from the International Tree-Ring Databank (Carr &  
262 Stahle, 2010; D. W. Stahle et al., 2010) (Figure 1). The bald cypress data included earlywood,  
263 latewood, and total ring width measurements, and we calculated a  $LW_{reg}$  series for each  
264 measurement series following the same methods as used for the longleaf pine (Griffin et al.,  
265 2011). Initial analyses indicated a common signal shared by the bald cypress trees from the two  
266 sites, which were therefore combined into a single set of measurement series for chronology  
267 development. In all, the bald cypress ring-width data included 74 measurement series from 34  
268 trees and spanned 1516–2005, with an  $EPS > 0.85$  from 1650–2005 (Figure 3c). The bald cypress  
269 ring-width data exhibited few synchronous disturbance events and were therefore standardized to

270 develop eight total chronologies—four STD created using splines of 50% frequency cutoff at  
271 100-year frequency to retain low-frequency growth patterns that could be linked to multi-decadal  
272 climate variability and four RES chronologies (TADI100; Figure 3c).

273

274 The complete set of chronologies included 16 longleaf pine chronologies and 8 bald cypress  
275 chronologies, each of which were clipped to the first year of a 50-yr window where the  
276 expressed population signal was  $>0.85$  (Wigley et al., 1984) to ensure a robust signal for climate  
277 and growth analyses (Figure 3b, 3c). The standardization process was carried out using the  
278 computer program Arstan v44xp (Cook & Krusic, 2013).

279



280

281 **Figure 3.** Linking tree growth to groundwater elevation. (a) Raw ring-width measurements of  
 282 the 172 ring-width series from 91 longleaf pine trees and stumps sampled at Goethe State Forest,  
 283 here normalized to a series mean of 0 with the sample-set mean shown in dark brown to illustrate  
 284 a deep suppression that spanned the 1890s into the early 1900s that was followed by a sharp  
 285 growth release that together likely represent land use changes associated with logging and  
 286 turpentine operations at the site. (b) Two sets of standardized ring width-index chronologies for

287 the longleaf pine, here developed from total ring width, shown to illustrate the influence of land  
288 use on tree growth and how the applied standardization methods (GSF30 with its 30-year  
289 smoothing splines depicted in orange vs. GSF100 with its 100-year smoothing splines depicted  
290 in blue) retained more or less low-frequency information in the resulting chronologies;  
291 interannual chronology values are shown as thin lines with the chronologies smoothed using 15-  
292 year splines shown as bold; sample depth and expressed population signals indicate both  
293 chronologies are robust from 1505–2018 ( $EPS > 0.85$  where chronology lines are solid). (c) The  
294 standardized ring-width index chronology derived from bald cypress trees growing along the  
295 nearby Withlacoochee River (TADI100; green) shown as annual values (thin line) and smoothed  
296 with a 15-yr spline (bold line), EPS ( $EPS > 0.85$  where chronology lines are solid), and sample  
297 depth. (d) Correlation coefficients (symbol) and confidence intervals (whiskers) between mean  
298 annual groundwater elevation and monthly PDSI, from year  $t-2$  to  $t$ , with bold colors indicating  
299 significant correlations ( $p < 0.05$ ). (e) Correlation coefficients and confidence intervals between  
300 each RWI chronology and monthly PDSI over the instrumental period, spanning from the  
301 previous year (lower case) to the current year (upper case), with bold colors indicating  
302 significant correlations ( $p < 0.05$ ). (f) Correlation coefficients between each of the total ring width  
303 RWI chronologies and mean monthly groundwater elevation over three years, from  $t$  to  $t+2$ , with  
304 bold colors indicating significant correlations ( $p < 0.05$ ).

305

## 306 2.4 Calibration, Verification, and Climate Reconstructions

307 Longleaf pine in this region of Florida are particularly sensitive to changes in hydrology because  
308 of the low water holding capacity of the sandy soils common to the region. Slight changes in  
309 depth to groundwater in such soils can have substantial effects on tree access to moisture

310 (Ciruzzi & Loheide, 2021; Foster & Brooks, 2001). Where access to groundwater does not  
311 directly impact tree growth, similar responses to precipitation and moisture balances may enable  
312 the identification of robust linkages between tree growth and groundwater elevation (Perez-  
313 Valdivia & Sauchyn, 2011). We therefore approached calibration of our tree-ring and  
314 groundwater data through a stepwise process that examined the environmental variables that  
315 could mechanistically link variability in tree growth and groundwater elevation. The  
316 relationships among these data were examined using correlation analyses as implemented in the  
317 `dcc()` function of the `treeClim` package of R (Zang & Biondi, 2015).

318  
319 First, we compared the relationships among instrumental climate data and groundwater  
320 variability through correlation analysis of both monthly and seasonal variables. The data used in  
321 this analysis included monthly precipitation, maximum temperature, and Palmer's Drought  
322 Severity Index (PDSI) time series from 1895–2017 for NCDC Florida Division 3 (NCDC, 2018),  
323 and groundwater elevation above the National Geodetic Vertical Datum of 1929 measured on the  
324 27th of each month near Newberry, Florida, at well S101722001 from 1959–2018 (Figure 1)  
325 (SRWMD, 2020). The USGS Newberry well was selected for its proximity to the study area and  
326 for the complete record it provided. The relationships among these data were examined for  
327 current and lagged relationships of up to two years using correlation analyses to identify links  
328 between atmospheric conditions and groundwater elevation. The strongest identified relationship  
329 between climate variables and groundwater elevation included a significant correlation between  
330 PDSI and groundwater elevation at up to a two-year lag, indicating persistence in the  
331 groundwater system (Figure 3d).

332

333 The climate responses of the 16 longleaf pine chronologies and 8 bald cypress chronologies  
334 exhibited similar overall relationships between tree growth and climate, with positive  
335 correlations to precipitation and PDSI and inverse relationships with maximum temperatures,  
336 though these varied by species and by the portion of the growth ring on which the chronologies  
337 were based (Figure S1). Differences in the seasonal timing of climate response were evident  
338 between EW and LW chronologies, and the window of climate response was narrower among  
339 the bald cypress chronologies than the longleaf pine chronologies (Figure S1). The strongest  
340 climate-growth relationships among all chronologies were consistently associated with PDSI  
341 (Figure 3e). This result supported the notion that soil moisture availability, as represented by  
342 PDSI, was directly related to both groundwater elevation and tree growth. Direct comparison of  
343 groundwater elevation and the tree-ring chronologies identified significant correlations that  
344 spanned windows of 8–25 months, with the strongest and most temporally expansive  
345 relationships identified with the longleaf pine chronologies (Figure 3f, Figure S2).

346  
347 Based on the observed relationships among climate, tree growth, and groundwater, we created a  
348 final set of predictors for a regression-based reconstruction by identifying the common variance  
349 among those tree-ring chronologies that showed significant correlations to groundwater  
350 elevation. First, all chronologies were clipped to include only the period where subsample  
351 strength was  $>0.85$ , indicating a robust signal suitable for reconstruction (Buras, 2017). We then  
352 assembled two separate matrices of tree-ring chronologies, one based on the GSF30 and  
353 TADI100 chronologies and one based only on the GSF100 chronologies. Persistence in the  
354 groundwater system that created lagged climate-groundwater relationships (Figure 3d) and tree  
355 physiology that resulted in lagged climate-growth relationships (Figure 3e) were accounted for

356 by lagging the chronologies in each matrix from  $t-4$  to  $t+4$ . The matrices were then refined by  
357 correlating each version of the chronologies with annual groundwater elevation at the USGS  
358 Newberry Well and retaining only those that exhibited significant Pearson product moment  
359 correlations ( $p < 0.01$ ). The first matrix spanned 1695–2002 and included 10 chronologies, five  
360 from the GSF30 and four from the TADI100 data sets. The second matrix spanned 1498–2015  
361 and included nine chronologies from the GSF100 data. We reduced the multicollinearity in each  
362 matrix using principle components analysis (PCA) as implemented by the `prcomp()` function in  
363 R (R Development Core Team, 2019).

364  
365 The principle components (PCs) derived for each matrix were considered in the development of  
366 two linear regression models using a forward and backward selection stepwise procedure as  
367 implemented in the `step()` function of R (R Development Core Team, 2019). The resulting  
368 reconstructions were assessed through a split calibration and verification process on the early and  
369 late halves of each calibration period using the `skill()` function in the R package `treeClim` (Zang  
370 & Biondi, 2015), rescaled to the instrumental record, and examined for potential bias using an  
371 extreme value capture test (McCarroll et al., 2015).

372  
373 The final GSF100 regression model explained 60% of the variance in mean annual instrumental  
374 groundwater elevation at the Newberry Well from 1959–2015, and the GSF30+TADI100  
375 reconstruction explained 60% of the variance in instrumental annual groundwater elevation from  
376 1959–2002 (Figure 4a). Both reconstructions were skillful, with reduction of error statistics of  
377 0.62–0.69 (Table 1). The coefficient of efficiency (CE) was positive in all cases, though it was  
378 close to zero when calibrated on the early split of the GSF100 reconstruction (Table 1). Of note,

379 when calibration and verification of the GSF100 reconstruction were conducted over the same  
380 period as the GSF30+TADI100 reconstruction (1959–2002), CE was strongly positive for both  
381 splits (see  $GSF100_{trim}$  in Table 1). Durbin-Watson  $d$  statistics were significant for all but the  
382 GSF100 late split based on the shortened calibration window which indicated significant  
383 autocorrelation in the model residuals. Visual inspection of the model showed the tree-ring  
384 reconstructions over-estimated groundwater elevation in more recent decades (Figure 4a).  
385 Comparing first-difference time series of both the instrumental and reconstructed time series  
386 indicated significant predictive power in the reconstructions even when trend was removed  
387 (Figure 4a). These results collectively indicate that useful information is provided by these  
388 reconstructions and also suggest the influence of a driving factor that affected groundwater  
389 elevation but not tree growth over the most recent decades.

390  
391 The two reconstructions were complementary. The reconstruction based on the  
392 GSF30+TADI100 chronologies did not extend as far into the past or as close to the present but  
393 retained low frequency variability most likely related to climate from the TADI100 chronologies,  
394 while the GSF30 chronologies contributed information about high-frequency variability with  
395 minimal influence of the late 1800s turpentine industry/land use signal (Figure 4b). The  
396 reconstruction based on the GSF100 chronologies extended further into the past and closer to the  
397 present, but due to the more conservative standardization retained low frequency variability in  
398 the late 1800s and early 1900s that represented land use influences and not climatic information  
399 (Figure 4b). Analysis of the extreme value capture (McCarroll et al., 2015) indicated that both  
400 the GSF30+TADI100 and the GSF100 reconstructions exhibited biases toward better  
401 representation of extreme high groundwater elevation ( $EVC = 3/4$  and  $4/6$ , respectively, both  $p <$

402 0.01) as compared to extreme low elevation (EVC = 2/4 and 2/6). This wet-bias is unusual  
403 among tree-ring-based hydrologic reconstructions that often better represent dry conditions  
404 (Wise & Dannenberg, 2019). This result could be explained by the persistence in groundwater  
405 elevations, where the relatively open groundwater aquifer created by the extremely well-drained  
406 sandy soils of the site may smooth out the effects of short-duration, extreme rainfall events that  
407 are often missed by trees growing in arid conditions. Alternatively, the asymmetry could be  
408 explained by non-climatic factors. All of the groundwater elevations within the 10<sup>th</sup> lowest  
409 percentile in the instrumental record occurred since 2001, the period of greatest potential impacts  
410 from groundwater extraction. Extreme lows in groundwater elevation driven in part by human  
411 factors would be absent in tree-ring records that more purely express climate drivers. Regardless  
412 of the reasons behind the asymmetrical extreme capture characteristics of the chronologies, the  
413 overall similarity in response of the two chronologies supported creation of a spliced  
414 reconstruction by adding the early and late portions of the GSF100 reconstruction onto the  
415 GSF30+TADI100 reconstruction. The resulting spliced chronology explained 63% of the  
416 variance in mean annual instrumental groundwater elevation and retained low-frequency signal  
417 throughout while minimizing the potential influence of land use in the 1800s (Figure 4a, 4c).  
418

419 As a final assessment of the spliced reconstruction, we compared the spatial footprints of  
420 instrumental and reconstructed groundwater elevation responses to drought and sea surface  
421 temperatures using KNMI Climate Explorer (Trouet & Van Oldenborgh, 2013). Spatial  
422 correlations with drought showed responses centered on northern Florida (Figure 5a), while  
423 correlations with sea surface temperatures depicted a clear relationship with El Niño-Southern  
424 Oscillation variability over the instrumental period (Figure 5b). Although both spatial signatures

425 were somewhat weaker with the reconstruction than the instrumental data, the geographic extent  
 426 and strength of the correlations were generally similar, broadly supporting the skill of the  
 427 reconstruction (Tegel et al., 2020).

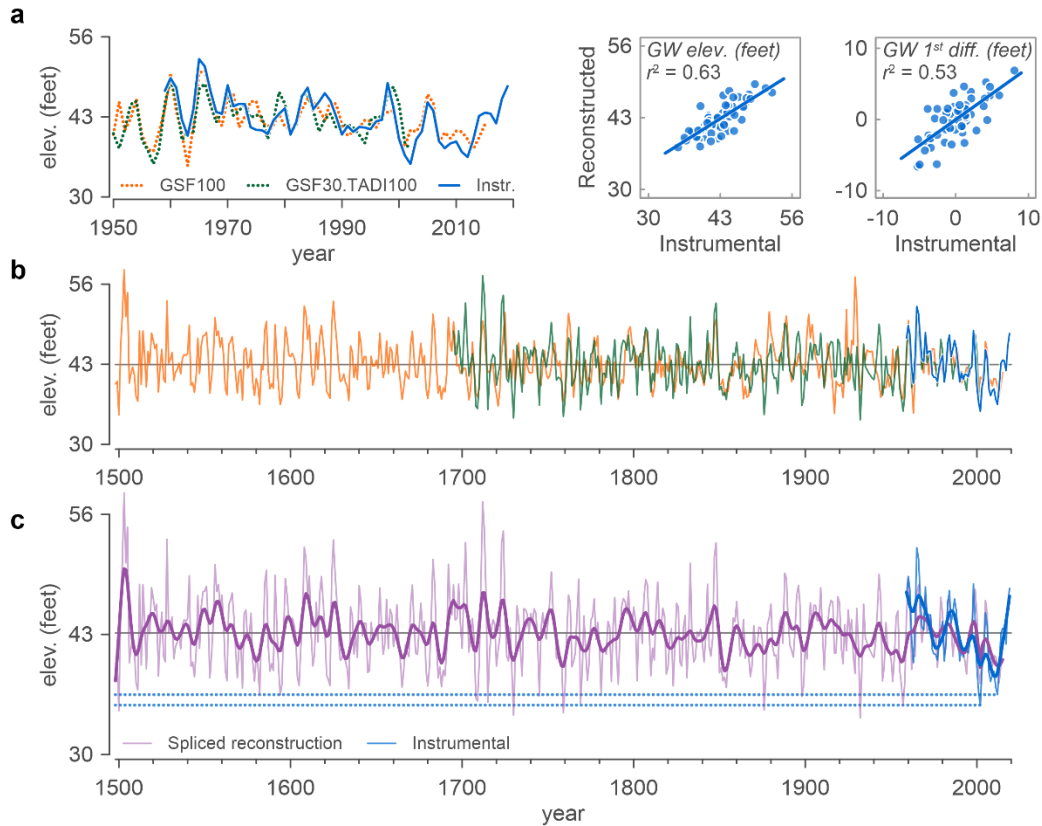
428

429 **Table 1.** Calibration and verification statistics for reconstructing mean annual groundwater  
 430 elevation in North Central Florida. The GSF100<sub>trim</sub> model results are based on the same  
 431 calibration window as the GSF30+TADI100 model. The spliced reconstruction includes the  
 432 GSF30+TADI100 model for years 1959–2002 and the GSF100 model for years 2003–2015.

Reconstruction	Calibration period	Validation period	$r^2$	RE	CE	$d$
GSF100	1959–2015		0.60			
	1959–1987	1988–2015	0.55	0.62	0.03	1.21*
	1988–2015	1959–1987	0.55	0.69	0.26	1.30*
GSF100 <sub>trim</sub>	1959–2002		0.57			
	1959–1980	1981–2002	0.57	0.61	0.26	1.04*
	1981–2002	1959–1980	0.61	0.53	0.52	1.71
GSF30+TADI100	1959–2002		0.60			
	1959–1980	1981–2002	0.64	0.62	0.45	0.99*
	1981–2002	1959–1980	0.50	0.69	0.56	0.90*
Spliced reconstruction	1959–2015		0.63			

433 \* indicates  $p < 0.05$

434



435

436 **Figure 4.** Calibration, verification, and reconstruction of mean annual groundwater elevation for

437 the Newberry USGS Well in North Central Florida. (a) Comparison of two versions of the

438 reconstruction (GSF100 only, GSF30+TADI100) with instrumental mean annual groundwater

439 elevation, along with scatter plots comparing the spliced reconstruction and instrumental

440 groundwater elevation. A similar scatter plot based on first-differenced versions of the

441 reconstruction and instrumental record is presented to specifically compare the high-frequency

442 patterns of the time series. (b) The full GSF100 and GSF30+TADI100 reconstructions along

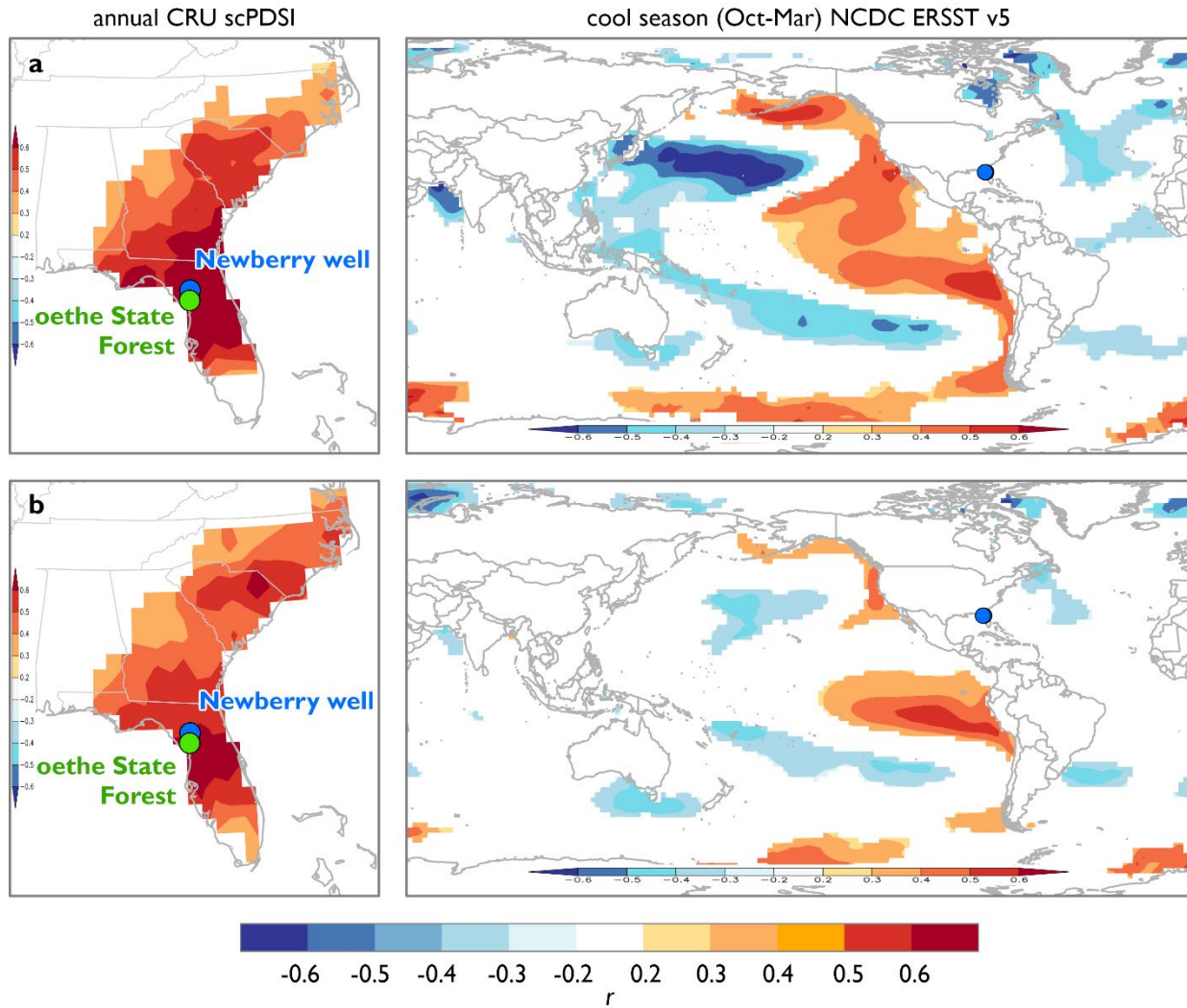
443 with the instrumental record. (c) The final spliced reconstruction shown relative to the

444 instrumental record, both with 15-yr smoothing splines to emphasize lower-frequency variations

445 in groundwater elevation. Thin horizontal dotted lines are included to compare extreme

446 individual-year lows in the instrumental record to the longer-term reconstruction.

447



448

449 **Figure 5.** Spatial climate response of instrumental and reconstructed groundwater elevation.

450 Correlation of (a) instrumental and (b) reconstructed annual groundwater elevation with drought

451 (scPDSI, 1959–2015) and sea surface temperatures (ERSST v5, 1977–2015). Correlations with

452 sea surface temperatures were stratified based on shifting relationships with ocean conditions

453 over time, as detailed below.

454

## 455 2.5 Interpreting the reconstruction: long-term variability in groundwater resources

456 The spliced reconstruction of mean annual groundwater elevation at the USGS Newberry well  
457 presented here extends information on groundwater elevation over 450 years beyond the  
458 instrumental record of the well, and over 400 years beyond any instrumental groundwater record  
459 in Florida. This expanded temporal perspective allows modern events to be viewed in the context  
460 of long-term variability; however, the calibration and verification results require additional  
461 consideration regarding the differing CE results for the GSF100 reconstruction when the most  
462 recent two decades are included in the calibration and the significant residuals in each version of  
463 the reconstruction. Comparing groundwater elevations recorded at the USGS Newberry well to  
464 those recorded at the Cross City well supports the notion that these results represent a dampening  
465 of the linkages that connect atmospheric conditions, tree rings, and groundwater elevations as the  
466 influences of groundwater extraction increase.

467

468 The Cross City well is located at the landward edge of Florida's Big Bend coastal zone, which,  
469 until somewhat recently, has been one of the least developed coastal regions of the United States  
470 (Volk et al., 2017). The Cross City well is thus more distant from urban centers and areas of  
471 intense agricultural groundwater use, making it less likely to be influenced by groundwater  
472 extraction (Figure 1), and while the numerous missing observations early in the record limit its  
473 usefulness as a target for calibration and reconstruction, the data do offer insight for interpreting  
474 the Newberry reconstruction. Comparing z scores for instrumental mean annual groundwater  
475 elevations at the Cross City and Newberry wells identifies an increasing difference between  
476 groundwater elevations at the two sites over time that is more pronounced during years of low  
477 groundwater (Figure 6a, 6b). This pattern matches both observed and modeled impacts of

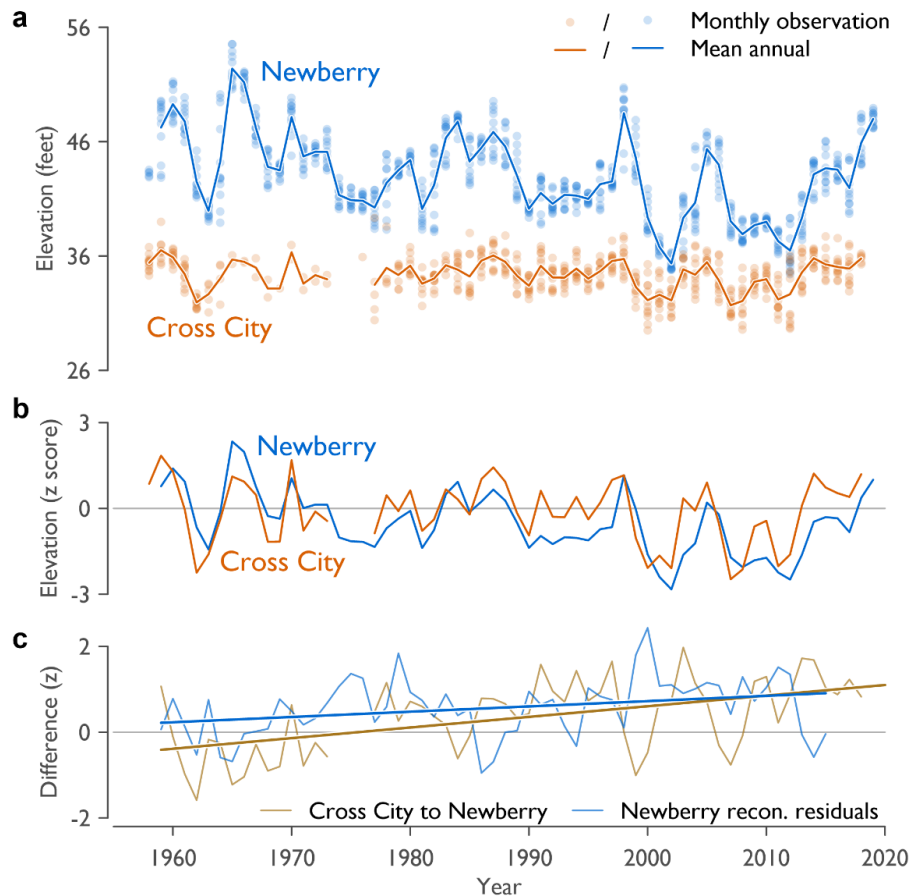
478 groundwater withdrawals on regional groundwater elevations (Gordu & Nachabe, 2021).  
479 Comparing the difference between the two well records to the Newberry reconstruction  
480 residuals, with both transformed into z scores, shows a similar increasing trend over time (Figure  
481 6c). Taken together, and in the context of known increases in groundwater extraction (Marella &  
482 Berndt, 2005), the increasing difference between groundwater elevation at the Cross City and  
483 USGS Newberry wells and the overestimation of recent groundwater elevation in the Newberry  
484 reconstruction represent a weakening of climatic control over groundwater elevation that is likely  
485 unprecedented. This also suggests that future low groundwater elevation will be amplified by  
486 groundwater extraction, increasing the probability of water resource scarcity beyond what has  
487 been experienced in at least the past 500 years.

488

489 The implications for interpreting the overall reconstruction are substantial, but do not undermine  
490 the value of the results reported here. Given the relatively recent development of high-capacity  
491 wells in the vicinity of the USGS Newberry well, and supported by data from modeling efforts, it  
492 is likely that substantial human impacts on groundwater elevation began in the 1990s and have  
493 increased since that time (Gordu & Nachabe, 2021). This means the calibration dataset provides  
494 at least three decades of relatively stable relationships among climate, groundwater elevation,  
495 and tree growth. The weakening of these relationships and amplified declines in groundwater  
496 elevation over recent decades, when included in the calibration and particularly when used to  
497 rescale the reconstruction, could bias the overall mean of the reconstruction. However, the strong  
498 relationship between the first-differenced instrumental and reconstructed time series and the  
499 similar spatial climate responses suggest that the reconstruction accurately captures interannual  
500 variability in groundwater elevation. Based on the assumption of stable climate-groundwater-tree

501 growth relationships prior to the period of groundwater extraction, we suggest that the  
 502 reconstruction presented here is a valid representation of pre-instrumental groundwater elevation.

503



504

505 **Figure 6.** Groundwater elevations at two wells in North Central Florida illustrate regionally  
 506 declining groundwater levels. (a) Observed mean annual groundwater elevations at the USGS  
 507 Newberry and Cross City wells. (b) Z scores of mean annual groundwater elevations for both  
 508 wells illustrating how the USGS Newberry instrumental measurements trend lower than those of  
 509 the Cross City well since ca. 1990. (c) Trend in the difference between instrumental groundwater  
 510 elevations at the Cross City well and the USGS Newberry well are similar to the Newberry  
 511 reconstruction residuals, reflecting the possible impacts of extraction on groundwater elevations  
 512 at the USGS Newberry well.

513 Given the considerations outlined above, the reconstruction of mean annual groundwater  
514 elevation at the USGS Newberry well provides important historical context for modern  
515 hydrologic conditions. First, as is the case with nearly all proxy-based hydrologic  
516 reconstructions, the distribution of reconstructed annual groundwater elevation for the  
517 instrumental period does not match the range of conditions represented over the full length of the  
518 reconstruction (Figure 7a). Reconstructed single year extreme lows and highs surpass the most  
519 extreme conditions observed since the start of direct groundwater elevation monitoring (Table 2)  
520 and suggest caution in basing long-term forecasts of water availability on the historical record  
521 (Pederson et al., 2012). Individual years and extended pluvial conditions in the mid-1500s, early  
522 1600s, and early 1700s exhibited higher groundwater elevations than experienced at any point in  
523 the instrumental period. At the same time, the low instrumental groundwater elevations recorded  
524 in 2002 and 2012 are among the lowest 5% of reconstructed groundwater elevations in the past  
525 500 years (Figure 4c, Table 2). The same years in the reconstruction are within the lowest 6%,  
526 and 15%, respectively—low, but not as extreme.

527

528 The more extreme ranking of these years based on instrumental records may be related to the  
529 extreme capture characteristics of the reconstruction, in that proxy-based records do not readily  
530 represent the most extreme conditions of the target variable (McCarroll et al., 2015). If that is the  
531 case, it would suggest that past lows in groundwater elevation in the reconstruction  
532 underestimate actual elevation and therefore serve as a conservative estimation of worst-case  
533 conditions. An alternative interpretation is that the reconstruction accurately represents the  
534 climatological influences on groundwater elevation and that groundwater extraction amplified  
535 these lows to extreme levels over recent decades. If true, this suggests that not only are the return

536 of extreme low groundwater conditions unavoidable due to climate variability, but that these  
537 conditions will be amplified by current and ongoing groundwater extraction. This increases the  
538 likelihood of North Central Florida experiencing more severe water deficits than experienced in  
539 the instrumental period thus far.

540

541 Building on the perspective gained from individual years, considering the consecutive number of  
542 years of above or below average groundwater elevation, or runs, provides a useful perspective on  
543 the duration of high- or low-groundwater conditions. We calculated runs relative to the mean of  
544 the full reconstruction ( $\bar{x} = 43.14$  feet above the National Geodetic Vertical Datum of 1929 from  
545 1498–2015) as a way to further place recent groundwater elevations in a long-term context  
546 (Figure 7b). The median run length was 2 years for both above- and below-average groundwater  
547 elevations, suggesting ground water elevations were primarily characterized by high-frequency  
548 variability; however, this was not consistent through time. Periods of more persistent above- and  
549 below-average conditions occurred at several points in the reconstruction, including from the  
550 mid-1500s through the early 1600s, and at approximately 50–70-year intervals from ca. 1700  
551 through 2000 (Figure 7b). The longest distinct run for above-average conditions relative to the  
552 long-term record was 10 years long and spanned 1791–1801, while the longest below-average  
553 runs included two 9-year periods of low groundwater from 1989–1997 and from 2007–2015.

554

555 Shifting levels of persistence in the reconstruction suggests shifting climate drivers of  
556 groundwater elevation. To supplement the runs analysis, we examined the power spectra of the  
557 reconstruction using a continuous Morlet wavelet transform calculated by the `morlet()` function  
558 in `dplr` (Bunn, 2008; Torrence & Compo, 1998). Significant periodicities at 5–15 years

559 identified throughout the 1500s into the early 1600s, again in the late 1600s into the mid-1700s,  
560 and sporadically throughout the 1800s and 1900s (Figure 7c) generally align with the periods of  
561 greater persistence identified in the runs analysis (Figure 7b). Significant periodicity in the ca.  
562 100-year band is evident from the 1600s through the 1900s and again aligns with peaks in  
563 persistence in the runs analysis centered on the years 1600, 1700, 1800, 1900, and possibly 2000.  
564 Interpretation of this response is problematic as frequencies above 100 years were largely  
565 removed from the tree-ring chronologies via standardization (Figure 7c). Collectively,  
566 interpretation of the runs and wavelet spectra suggest an important role in groundwater  
567 elevations for climate drivers that exhibit oscillatory behaviors, but that the influences of these  
568 factors wax and wane through time.

569  
570 The expression of shifting persistence in groundwater elevation variability is illustrated by  
571 considering cumulative anomalies, defined here as the sum of annual groundwater elevation  
572 anomalies over continuous periods of above- or below-average groundwater elevation relative to  
573 the reconstruction mean. Periods of low persistence such as those in the mid-1600s and early  
574 1800s generally aligned with near-average groundwater elevations, while periods of greater  
575 persistence coincided with deep pluvial or drought conditions (Figure 7d). For example,  
576 cumulative anomalies of below-average groundwater elevations clustered in the late 16<sup>th</sup> century,  
577 which is a period of megadrought documented across much of North America (David W. Stahle  
578 et al., 2007). In this context, recent cumulative anomalies of below-average groundwater  
579 elevations, driven in part by the rise in persistence over recent decades, were surpassed only once  
580 in the past 500 years (Figure 7c, 7d). Furthermore, the overestimation of groundwater elevation  
581 for recent decades of the reconstruction (Figure 6) suggests that while hydrologic drought

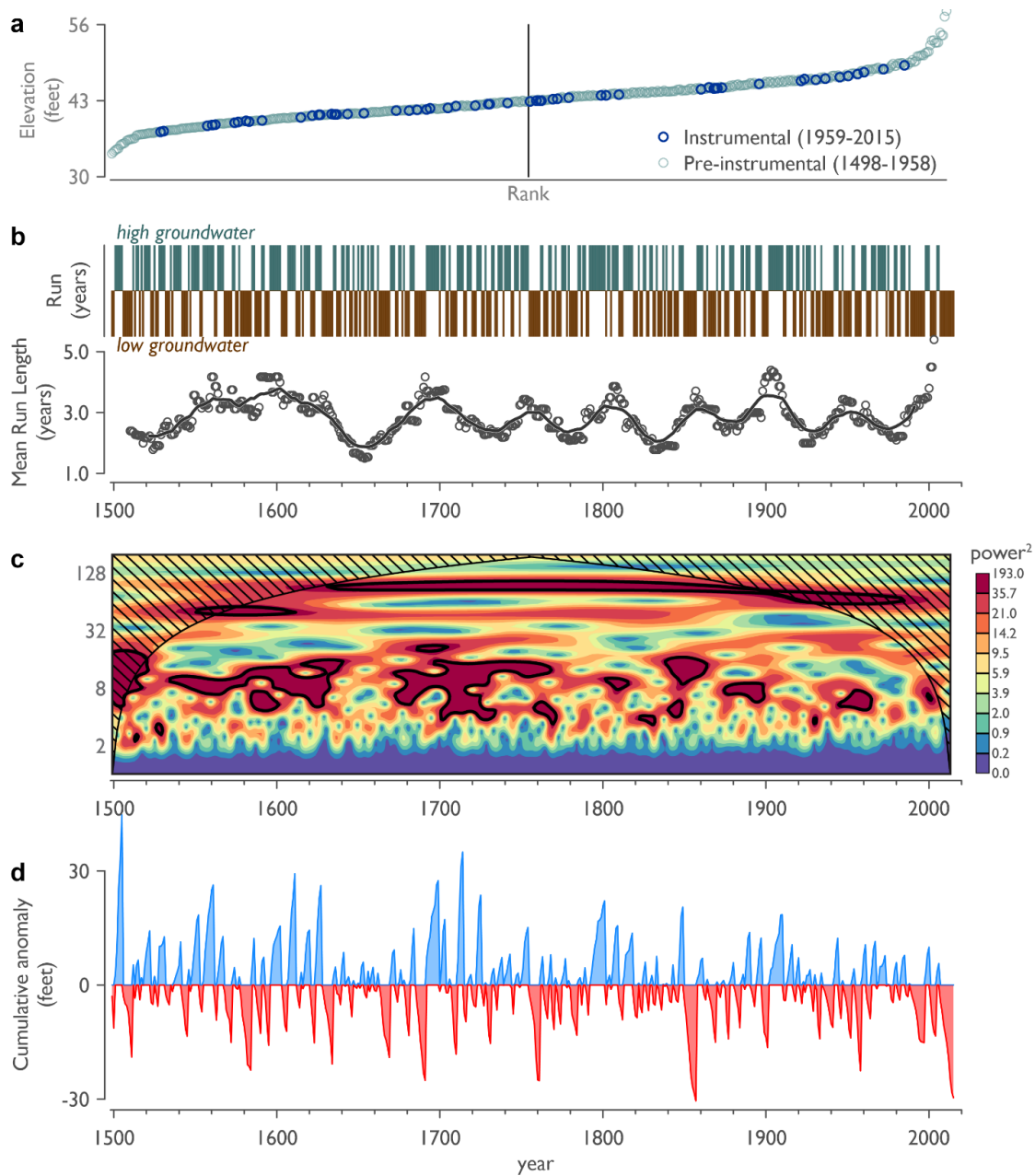
582 contributed to recent declines in groundwater elevation across the southeastern United States  
 583 (Vines et al., 2021), the potential amplification of these declines by groundwater extraction likely  
 584 resulted in the some of the lowest groundwater elevations in at least the past 500 years (Figure  
 585 4c, 7d).

586

587 **Table 2.** Years of extreme reconstructed groundwater elevations

Years of extreme low groundwater				Years of extreme high groundwater			
Reconstructed		Observed		Reconstructed		Observed	
year	Elevation (ft)	year	Elevation (ft)	year	Elevation (ft)	year	Elevation (ft)
1932	34.0	2002	35.4	1503	58.3	1965	52.4
1730	34.3	2012	36.5	1712	57.4	1966	51.2
1759	34.5	2001	36.8	1724	54.2	1960	49.3
1500	34.8	2011	37.3	1713	54.1	1998	48.5
1876	34.8	2008	37.9	1505	54.6	1970	48.1
1957	35.4	2009	38.7	1702	52.9	2019	48.0
1769	35.6	2010	39.0	1848	52.9	1961	47.8
1715	35.6	2007	39.0	1723	52.9	1984	47.7
1709	35.8	2003	39.3	1528	53.3	1959	47.2
1708	36.2	2013	39.3	1625	53.2	1967	47.2
1898	36.3	2000	39.4	1608	52.5	1987	46.8
1745	36.4	1963	40.0	1847	51.4	1983	46.3
1594	36.5	1981	40.1	1609	51.3	2018	45.9
1582	36.5	1990	40.1	1683	51.1	1988	45.6
1781	36.5	1977	40.2	1833	50.7	1986	45.5

588



589

590 **Figure 7.** Analysis of reconstructed groundwater elevation. (a) A ranked distribution of  
 591 groundwater elevation depicting the reconstructed values during the instrumental period relative  
 592 to the entire reconstruction. (b) Runs of consecutive years above- or below-average groundwater  
 593 elevations relative to the mean of the full reconstruction (1498–2015) shown as unique events  
 594 (top) and as a moving 25-yr average of the length of each run, regardless of the associated sign,  
 595 fit with a 25-year moving average for illustration purposes. (c) Wavelet power spectra of the

596 spliced groundwater reconstruction for North Central Florida. Black contours indicate significant  
597 power ( $p < 0.05$ ). Cross-hatched regions are the cone of influence where spectra may be distorted  
598 due to edge effects. (d) Cumulative anomalies shown as the sum of consecutive anomalies in  
599 each run of above- or below-average groundwater elevations.

600

601

602 2.6 Considering the influences of oceanic-atmospheric phenomena on groundwater

603 In Florida, multiple oceanic-atmospheric phenomena interact to influence patterns of  
604 atmospheric circulation that, in turn, drive hydrological variability and groundwater conditions.

605 These include the El Niño-Southern Oscillation (ENSO) and the Atlantic Multidecadal

606 Oscillation (AMO), both of which may be modulated through interactions with sea surface

607 temperatures in the north Pacific (Enfield et al., 2001; McCabe et al., 2008; McCabe et al., 2004;

608 Tootle & Piechota, 2006). Although the impacts of these phenomena are documented over the

609 instrumental record, their influence on the climate of northern Florida is variable over time,

610 particularly with respect to ENSO (Cole & Cook, 1998; Torbenson et al., 2019). The significant

611 band of 5–15 year periodicity identified through much of the reconstruction encapsulates ENSO-

612 scale forcing (Cane, 1986), as well as longer-term variability, while the 100-yr periodicity

613 identified in the reconstruction surpasses the canonical description of AMO variability (Enfield

614 et al., 2001; Newman et al., 2016). It is noteworthy that neither of these modes of variability in

615 the reconstruction precisely fit the observed scale at which these coupled oceanic-atmospheric

616 phenomena operate, and yet consistent patterns of increasing and decreasing persistence exist in

617 the reconstruction that reflect the oscillatory behavior associated with these processes. This

618 suggests the existence of inter-basin interactions of oceanic-atmospheric processes that drive the

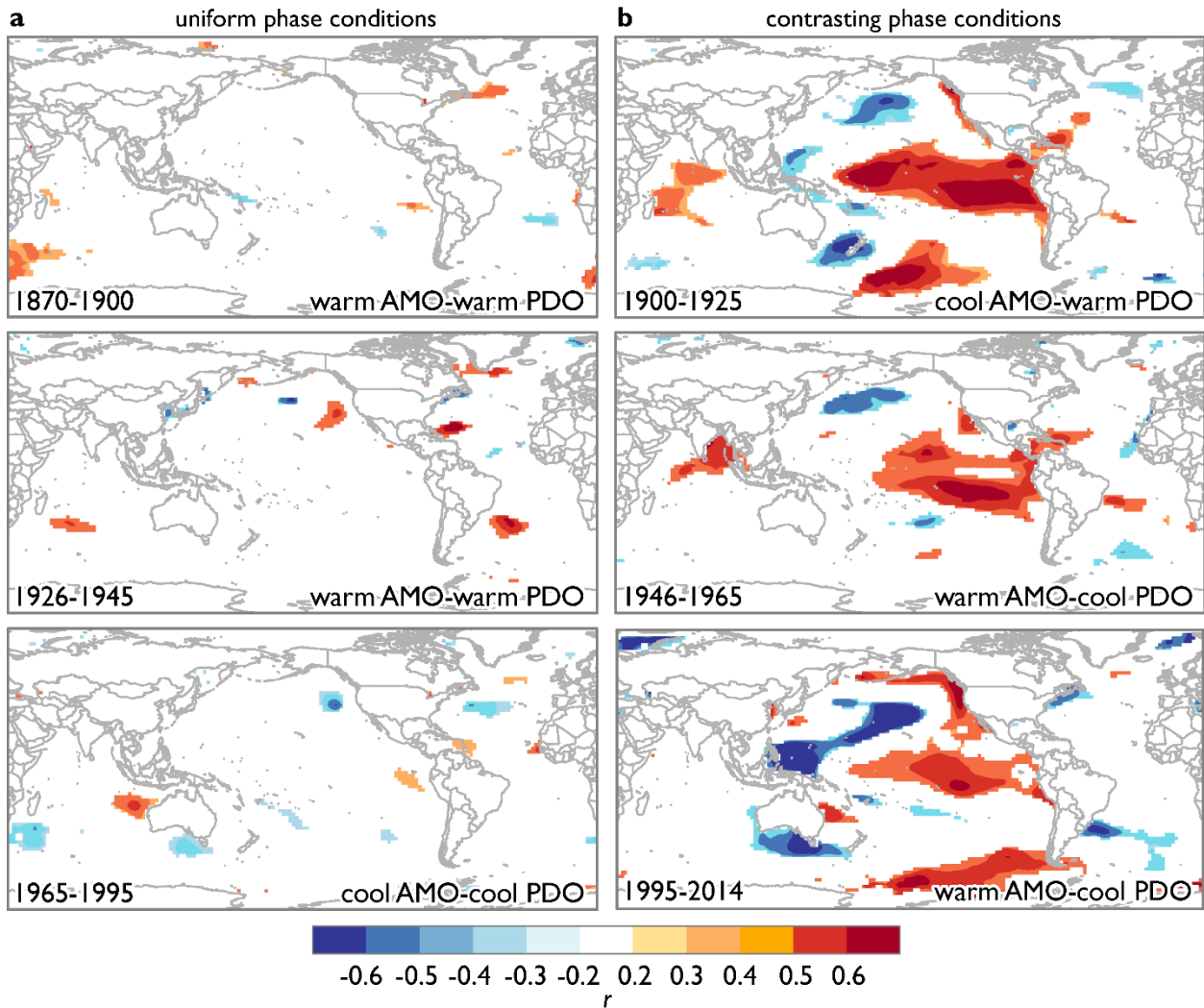
619 periodicity and variable persistence in groundwater elevations at our site. This is illustrated by  
620 examining the relationship between the reconstruction and global sea surface temperatures over  
621 time.

622

623 Correlations between the groundwater reconstruction and global SST (NCDC ERSST v5, Huang  
624 et al., 2017), calculated and visualized using KNMI Climate Explorer (Trouet & Van  
625 Oldenborgh, 2013), illustrate modulation of ENSO influences over time by contingent phases of  
626 the AMO and PDO (Dong et al., 2006; Li et al., 2013; Yeh & Kirtman, 2005). The influence of  
627 ENSO on groundwater elevation was strongest during periods of contrasting AMO and PDO  
628 phases and diminished during periods of coherent phases of these coupled oceanic-atmospheric  
629 phenomena (Figure 8). The temporal scope of this analysis was extended beyond the period of  
630 instrumental sea surface temperature records by comparing the groundwater elevation  
631 reconstruction to a suite of proxy-based reconstructions of ENSO variability that were variously  
632 based on tree-ring and coral records (Datwyler et al., 2019; Freund et al., 2019; Li et al., 2013;  
633 D. W. Stahle et al., 1998; Torbenson et al., 2019). Moving correlations over 25-year windows  
634 indicated widely varying relationships between groundwater elevation and each representation of  
635 ENSO activity (Figure 9). Taken together, these results underscore that northern Florida is within  
636 a region of intersection among multiple climate driver impacts (Maleski & Martinez, 2018), and  
637 that while this produces inconsistent patterns of teleconnection influences through time, the  
638 longer-term perspective of groundwater elevations enabled through this tree-ring-based  
639 reconstruction helps identify patterns in groundwater conditions that may prove helpful for  
640 groundwater resource projects. Specifically, understanding how the sea surface temperatures  
641 associated with contrasting phases of the AMO and PDO influence atmospheric circulation to

642 amplify ENSO influences on groundwater resources in northern Florida could enable forecasting  
 643 persistence and the likelihood of long-term water abundance or scarcity.

644

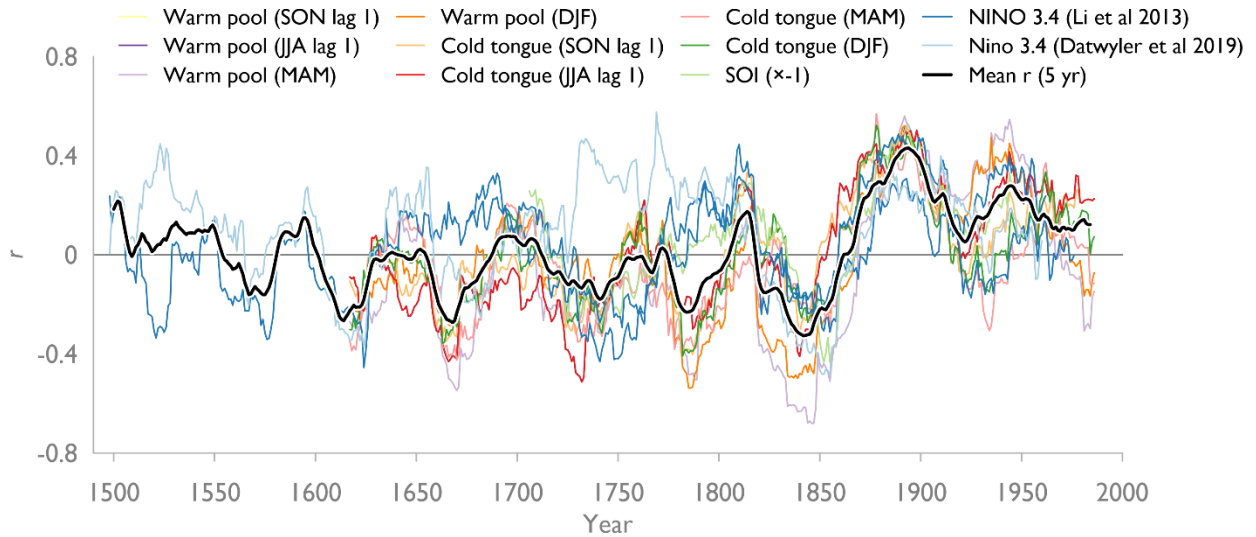


645

646

647 **Figure 8.** Shifting relationships between sea surface temperatures (SST) and reconstructed  
 648 groundwater elevation in North Central Florida. Correlations between annual groundwater  
 649 elevation and December–March NCDCE ERSST v5 sea surface temperatures during (a) periods of  
 650 similar AMO and PDO phases and (b) periods of contrasting AMO and PDO phases illustrate a  
 651 temporally variable influence of ENSO on North Central Florida hydrologic conditions.

652



653

654 **Figure 9.** Relationship between reconstructed North Central Florida groundwater and a suite of

655 proxy-based reconstructions of different aspects of El Niño-Southern Oscillation variability.

656 Values are the Pearson product moment correlation coefficient for the first year of moving 30-

657 year windows.

658

659

### 660 3. Conclusions

661 The reconstruction we report here expands tenfold the temporal perspective on groundwater

662 variability in North Central Florida. In doing so, we identified a high likelihood of recent low

663 groundwater elevations that reached levels comparable to past megadrought periods and suggest

664 that groundwater extraction likely magnified the influence of climate to drive these extreme

665 lows. Collectively, our results illustrate the cross-scale interactions of inter-basin oceanic-

666 atmospheric teleconnections that modulate the influence of ENSO variability on northern Florida

667 hydroclimate variability. These climate drivers create periods of greater and less persistence

668 within groundwater elevations that in turn produce prolonged periods of near-average conditions  
669 when persistence is low and pluvial or deep drought when persistence is high. Based on the past  
670 500 years of groundwater elevations, it appears that persistence is currently increasing and will  
671 likely do so for at least another decade. This suggests that water resource managers would do  
672 well to plan for sustained conditions that could continue current droughts or cause a switch to a  
673 prolonged pluvial. The amplification of future drought conditions by groundwater extraction will  
674 lead to water scarcity at levels not observed during the instrumental period.

675

#### 676 **Acknowledgments**

677 Thanks go to Nick Flinner for his steadfast work developing initial tree-ring chronologies from  
678 old longleaf pine stumps, Zach Holmboe and Sam Horsnell for their assistance in the field, Fay  
679 Baird for help in the field and gathering and collating groundwater well data, and Mark Larson  
680 for his assistance in identifying sampling areas and understanding the history of Goethe State  
681 Forest. Neil Pederson provided insightful comments on an earlier version of this manuscript that  
682 helped refine our approach to reconstructing groundwater variability. Funding for this research  
683 was provided by the Suwannee River Water Management District. The authors declare no real or  
684 perceived conflicts of interest.

685

#### 686 **Open Research**

687 Upon acceptance for publication, all tree-ring data developed for this study will be made publicly  
688 accessible through the International Tree-Ring Data Bank [available:  
689 <https://www.ncei.noaa.gov/products/paleoclimatology/tree-ring>], with the following statement  
690 then relevant:

691  
692 The tree-ring data used in the groundwater reconstruction are available at the International Tree-  
693 Ring Data Bank (<https://www.ncei.noaa.gov/products/paleoclimatology/tree-ring>) via [link;  
694 Goethe State Forest longleaf pine chronologies], [link2; Bald cypress chronologies], and [link3;  
695 Bald cypress chronologies]. Instrumental groundwater data used are available through the My  
696 Suwannee River Water Management District portal  
697 (<https://www.mysuwanneeriver.com/108/Groundwater-Levels>) via  
698 [[http://www.mysuwanneeriver.org/data/GWData/S101722001/S101722001\\_Level.xlsx](http://www.mysuwanneeriver.org/data/GWData/S101722001/S101722001_Level.xlsx);  
699 Newberry] and  
700 [[http://www.mysuwanneeriver.org/data/GWData/S101210001/S101210001\\_Level.xlsx](http://www.mysuwanneeriver.org/data/GWData/S101210001/S101210001_Level.xlsx); Cross  
701 City]. Figures were created using Grapher v15 software (<https://www.goldensoftware.com>) and  
702 maps were created in ArcGIS Pro v2.4 (<https://www.esri.com>).

703

704

## 705 **References**

706 Barlow, P. M. (2003). *Ground Water in Freshwater-Saltwater Environments of the Atlantic Coast.*

707 Reston, Virginia: U.S. Geological Survey Circular 1262.

708 BEBR. (2011). *Florida estimates of population 2010*. Retrieved from University of Florida Bureau

709 of Economic and Business Research, Gainesville, Florida:

710 [https://www.behr.ufl.edu/population\\_repo\\_cats/florida-population-estimates/](https://www.behr.ufl.edu/population_repo_cats/florida-population-estimates/)

711 BEBR. (2020). *Florida estimates of population 2020*. Retrieved from University of Florida Bureau

712 of Economic and Business Research, Gainesville, Florida:

713 [https://www.behr.ufl.edu/population\\_repo\\_cats/florida-population-estimates/](https://www.behr.ufl.edu/population_repo_cats/florida-population-estimates/)

- 714 Bierkens, M. F. P., & Wada, Y. (2019). Non-renewable groundwater use and groundwater  
715 depletion: a review. *Environmental Research Letters*, *14*(6), 063002.  
716 <https://doi.org/10.1088/1748-9326/ab1a5f>
- 717 Bunn, A. G. (2008). A dendrochronology program library in R (dplR). *Dendrochronologia*, *26*,  
718 115–124. <https://doi.org/10.1016/j.dendro.2008.01.002>
- 719 Buras, A. (2017). A comment on the expressed population signal. *Dendrochronologia*, *44*, 130–  
720 132. <https://doi.org/10.1016/j.dendro.2017.03.005>
- 721 Cane, M. A. (1986). El Niño. *Annual Review of Earth and Planetary Sciences*, *14*, 43–70.  
722 <https://doi.org/10.1146/annurev.ea.14.050186.000355>
- 723 Carr, D., & Stahle, D. W. (2010). *NOAA/WDS Paleoclimatology - Carr - Middle Withlacoochee*  
724 *River - TADI - ITRDB FL008*. NOAA National Centers for Environmental Information.  
725 <https://doi.org/10.25921/gqph-x765>. Accessed June 15, 2019.
- 726 Ciruzzi, D. M., & Loheide, S. P. (2021). Groundwater subsidizes tree growth and transpiration in  
727 sandy humid forests. *Ecohydrology*, *14*(5). <https://doi.org/10.1002/eco.2294>
- 728 Cole, J. E., & Cook, E. R. (1998). The changing relationship between ENSO variability and  
729 moisture balance in the continental United States. *Geophysical Research Letters*, *25*(24),  
730 4529–4532. <https://doi.org/10.1029/1998GL900145>
- 731 Cook, E. R. (1985). *A Time Series Analysis Approach to Tree Ring Standardization*. (Ph.D. Ph.D.  
732 Dissertation), University of Arizona, Tucson, Arizona.
- 733 Cook, E. R., & Krusic, P. J. (2013). ARSTAN v44h2: A tree-ring standardization program based  
734 on detrending and autoregressive time series modeling, with interactive graphics.  
735 Palisades, New York, USA: Tree-Ring Laboratory, Lamont-Doherty Earth Observatory of  
736 Columbia University.

- 737 Cook, E. R., & Peters, K. (1981). The smoothing spline: a new approach to standardizing forest  
738 interior tree-ring width series for dendroclimatic studies. *Tree-Ring Bulletin*, 41, 45–53.  
739 <http://hdl.handle.net/10150/261038>
- 740 Cook, E. R., & Peters, K. (1997). Calculating unbiased tree-ring indices for the study of climatic  
741 and environmental change. *The Holocene*, 7(3), 361–370.  
742 <https://doi.org/10.1177/095968369700700314>
- 743 Crockett, K., Martin, J. B., Grissino-Mayer, H. D., Larson, E. R., & Mirti, T. (2010). Assessment  
744 of tree rings as a hydrologic record in a humid subtropical environment. *Journal of the*  
745 *American Water Resources Association*, 46(5), 919–931. [https://doi.org/10.1111/j.1752-](https://doi.org/10.1111/j.1752-1688.2010.00464.x)  
746 [1688.2010.00464.x](https://doi.org/10.1111/j.1752-1688.2010.00464.x)
- 747 Datwyler, C., Abram, N. J., Grosjean, M., Wahl, E. R., & Neukom, R. (2019). El Nino-Southern  
748 Oscillation variability, teleconnection changes and responses to large volcanic eruptions  
749 since AD 1000. *International Journal of Climatology*, 39(5), 2711–2724. Article.  
750 <https://doi.org/10.1002/joc.5983>
- 751 de Graaf, I. E. M., Gleeson, T., van Beek, L. P. H., Sutanudjaja, E. H., & Bierkens, M. F. P. (2019).  
752 Environmental flow limits to global groundwater pumping. *Nature*, 574(7776), 90–94.  
753 <http://dx.doi.org/10.1038/s41586-019-1594-4>
- 754 Dong, B. W., Sutton, R. T., & Scaife, A. A. (2006). Multidecadal modulation of El Niño-Southern  
755 Oscillation (ENSO) variance by Atlantic Ocean sea surface temperatures. *Geophysical*  
756 *Research Letters*, 33(8), L08705. Article. <https://doi.org/10.1029/2006gl025766>
- 757 Enfield, D. B., Mestas-Nunez, A. M., & Trimble, P. J. (2001). The Atlantic multidecadal  
758 oscillation and its relation to rainfall and river flows in the continental US. *Geophysical*  
759 *Research Letters*, 28(10), 2077–2080. <https://doi.org/10.1029/2000GL012745>

- 760 Ferguson, G., & St. George, S. (2003). Historical and estimated ground water levels near  
761 Winnipeg, Canada, and their sensitivity to climatic variability. *Journal of the American*  
762 *Water Resources Association*, 39(5), 1249–1259. Article. [https://doi.org/10.1111/j.1752-](https://doi.org/10.1111/j.1752-1688.2003.tb03706.x)  
763 [1688.2003.tb03706.x](https://doi.org/10.1111/j.1752-1688.2003.tb03706.x)
- 764 Foster, T. E., & Brooks, J. R. (2001). Long-term trends in growth of *Pinus palustris* and *Pinus*  
765 *elliottii* along a hydrological gradient in central Florida. *Canadian Journal of Forest*  
766 *Research*, 31(10), 1661–1670. <https://doi.org/10.1139/x01-100>
- 767 Freund, M. B., Henley, B. J., Karoly, D. J., McGregor, H. V., Abram, N. J., & Dommenges, D.  
768 (2019). Higher frequency of Central Pacific El Niño events in recent decades relative to  
769 past centuries. *Nature Geoscience*, 12(6), 450–455. Article.  
770 <https://doi.org/10.1038/s41561-019-0353-3>
- 771 Fritts, H. C. (1976). *Tree Rings and Climate*. New York: Academic Press.
- 772 Gholami, V., Torkaman, J., & Khaleghi, M. R. (2017). Dendrohydrogeology in  
773 paleohydrogeologic studies. *Advances in Water Resources*, 110, 19–28. Article.  
774 <https://doi.org/10.1016/j.advwatres.2017.10.004>
- 775 Gordu, F., & Nachabe, M. H. (2021). Hindcasting multidecadal predevelopment groundwater  
776 levels in the Floridan aquifer. *Groundwater*, 59(4), 524–536. Article.  
777 <https://doi.org/10.1111/gwat.13073>
- 778 Griffin, D., Meko, D. M., Touchan, R., Leavitt, S. W., & Woodhouse, C. A. (2011). Latewood  
779 chronology development for summer-moisture reconstruction in the US Southwest. *Tree-*  
780 *Ring Research*, 67(2), 87–101. <https://doi.org/10.3959/2011-4.1>
- 781 Harley, G. L., Maxwell, J. T., Larson, E., Grissino-Mayer, H. D., Henderson, J., & Huffman, J.  
782 (2017). Suwannee River flow variability 1550–2005 CE reconstructed from a multispecies

- 783 tree-ring network. *Journal of Hydrology*, 544, 438–451.  
784 <http://dx.doi.org/10.1016/j.jhydrol.2016.11.020>
- 785 Huang, B., Thorne, P. W., Banzon, V. F., Boyer, T., Chepurin, G., Lawrimore, J. H., et al. (2017).  
786 Extended reconstructed sea surface temperature, version 5 (ERSSTv5): Upgrades,  
787 validations, and intercomparisons. *Journal of Climate*, 30(20), 8179–8205.  
788 <https://doi.org/10.1175/jcli-d-16-0836.1>
- 789 Huffman, J. M., & Rother, M. T. (2017). Dendrochronological field methods for fire history in  
790 pine ecosystems of the Southeastern Coastal Plain. *Tree-Ring Research*, 73(1), 42–46.  
791 <https://doi.org/10.3959/1536-1098-73.1.42>
- 792 Hunter, S. C., Allen, D. M., & Kohfeld, K. E. (2020). Comparing approaches for reconstructing  
793 groundwater levels in the mountainous regions of interior British Columbia, Canada, using  
794 tree ring widths. *Atmosphere*, 11(12), 25. Article. <https://doi.org/10.3390/atmos11121374>
- 795 Jasechko, S., & Perrone, D. (2021). Global groundwater wells at risk of running dry. *Science*,  
796 372(6540), 418-+. Article. <https://doi.org/10.1126/science.abc2755>
- 797 Li, J. B., Xie, S. P., Cook, E. R., Morales, M. S., Christie, D. A., Johnson, N. C., et al. (2013). El  
798 Niño modulations over the past seven centuries. *Nature Climate Change*, 3(9), 822–826.  
799 Article. <https://doi.org/10.1038/nclimate1936>
- 800 Maleski, J. J., & Martinez, C. J. (2018). Coupled impacts of ENSO AMO and PDO on temperature  
801 and precipitation in the Alabama–Coosa–Tallapoosa and Apalachicola–Chattahoochee–  
802 Flint river basins. *International Journal of Climatology*, 38(S1), e717–e728.  
803 <https://doi.org/10.1002/joc.5401>

- 804 Marella, R. L., & Berndt, M. P. (2005). *Water withdrawals and trends from the Floridan aquifer*  
805 *system in the southeastern United States, 1950-2000*. Reston, Virginia: U.S. Geological  
806 Survey Circular 1278.
- 807 McCabe, G. J., Betancourt, J. L., Gray, S. T., Palecki, M. A., & Hidalgo, H. G. (2008).  
808 Associations of multi-decadal sea-surface temperature variability with US drought.  
809 *Quaternary International*, 188, 31–40. Proceedings Paper.  
810 <https://doi.org/10.1016/j.quaint.2007.07.001>
- 811 McCabe, G. J., Palecki, M. A., & Betancourt, J. L. (2004). Pacific and Atlantic Ocean influences  
812 on multidecadal drought frequency in the United States. *Proceedings of the National*  
813 *Academy of Sciences of the United States of America*, 101(12), 4136–4141.  
814 <https://doi.org/10.1073/pnas.0306738101>
- 815 McCarroll, D., Young, G. H., & Loader, N. J. (2015). Measuring the skill of variance-scaled  
816 climate reconstructions and a test for the capture of extremes. *The Holocene*, 25(4), 618–  
817 626. <https://doi.org/10.1177/0959683614565956>
- 818 Meko, D. M. (1981). *Application of Box-Jenkins methods of time series analysis to the*  
819 *reconstruction of drought from tree rings*. (Ph.D. Ph.D. Dissertation), University of  
820 Arizona, Tucson, Arizona.
- 821 Miller, J. A. (1990). *Ground Water Atlas of the United States: Segment 6, Alabama, Florida,*  
822 *Georgia, South Carolina* (730G). Retrieved from  
823 <http://pubs.er.usgs.gov/publication/ha730G>
- 824 NCDC. (2018). Monthly Historical Climate Time Series. Retrieved from  
825 <https://www7.ncdc.noaa.gov/CDO/CDODivisionalSelect.jsp>

- 826 Newman, M., Alexander, M. A., Ault, T. R., Cobb, K. M., Deser, C., Lorenzo, E. D., et al. (2016).  
827 The Pacific Decadal Oscillation, revisited. *Journal of Climate*, 29(12), 4399–4427.  
828 <https://doi.org/10.1175/JCLI-D-15-0508.1>
- 829 Outland III, R. B. (2004). *Tapping the Pines: The Naval Stores Industry in the American South*.  
830 Baton Rouge, Louisiana: LSU Press.
- 831 Pederson, N., Bell, A. R., Knight, T. A., Leland, C., Malcomb, N., Anchukaitis, K. J., et al. (2012).  
832 A long-term perspective on a modern drought in the American Southeast. *Environmental*  
833 *Research Letters*, 7(1), 014034. <https://doi.org/10.1088/1748-9326/7/1/014034>
- 834 Perez-Valdivia, C., & Sauchyn, D. (2011). Tree-ring reconstruction of groundwater levels in  
835 Alberta, Canada: Long term hydroclimatic variability. *Dendrochronologia*, 29(1), 41–47.  
836 <http://dx.doi.org/10.1016/j.dendro.2010.09.001>
- 837 R Development Core Team. (2019). R: A language and environment for statistical computing  
838 (Version v2.11.1). Vienna, Austria: R Foundation for Statistical Computing. Retrieved  
839 from <http://www.R-project.org>
- 840 Schmidt, N., Lipp, E. K., Rose, J. B., & Luther, M. E. (2001). ENSO influences on seasonal rainfall  
841 and river discharge in Florida. *Journal of Climate*, 14(4), 615–628.  
842 [https://doi.org/10.1175/1520-0442\(2001\)014<0615:EIOSRA>2.0.CO;2](https://doi.org/10.1175/1520-0442(2001)014<0615:EIOSRA>2.0.CO;2)
- 843 SRWMD. (2020). Suwannee River Water Management District Groundwater Portal.
- 844 Stahle, D. W., Carr, D., Griffin, R. D., & Jennings, J. (2010). *NOAA/WDS Paleoclimatology -*  
845 *Stahle - Upper Withlacoochee River - TADI - ITRDB FL009*. NOAA National Centers for  
846 Environmental Information. <https://doi.org/10.25921/gqph-x765>. Accessed June 15, 2019.
- 847 Stahle, D. W., D'Arrigo, R., Krusic, P. J., Cleaveland, M. K., Cook, E., Allan, R. J., et al. (1998).  
848 Experimental dendroclimatic reconstruction of the Southern Oscillation. *Bulletin of the*

- 849 *American Meteorological Society*, 79(10), 2137–2152. [https://doi.org/10.1175/1520-](https://doi.org/10.1175/1520-0477(1998)079<2137:EDROTS>2.0.CO;2)  
850 [0477\(1998\)079<2137:EDROTS>2.0.CO;2](https://doi.org/10.1175/1520-0477(1998)079<2137:EDROTS>2.0.CO;2)
- 851 Stahle, D. W., Fye, F. K., Cook, E. R., & Griffin, R. D. (2007). Tree-ring reconstructed  
852 megadroughts over North America since A.D. 1300. *Climatic Change*, 83(1), 133–149.  
853 journal article. <https://doi.org/10.1007/s10584-006-9171-x>
- 854 Sutton, C., Kumar, S., Lee, M. K., & Davis, E. (2021). Human imprint of water withdrawals in the  
855 wet environment: A case study of declining groundwater in Georgia, USA. *Journal of*  
856 *Hydrology-Regional Studies*, 35, 16. Article. <https://doi.org/10.1016/j.ejrh.2021.100813>
- 857 Tegel, W., Seim, A., Skiadaresis, G., Ljungqvist, F., Kahle, H.-P., & Land, A. (2020). Higher  
858 groundwater levels in western Europe characterize warm periods in the Common Era.  
859 *Scientific Reports*, 10. <https://doi.org/10.1038/s41598-020-73383-8>
- 860 Tootle, G. A., & Piechota, T. C. (2006). Relationships between Pacific and Atlantic ocean sea  
861 surface temperatures and U.S. streamflow variability. *Water Resources Research*, 42(7),  
862 W07411. <https://doi.org/10.1029/2005wr004184>
- 863 Torbenson, M. C. A., Stahle, D. W., Howard, I. M., Burnette, D. J., Villanueva-Diaz, J., Cook, E.  
864 R., & Griffin, D. (2019). Multidecadal modulation of the ENSO teleconnection to  
865 precipitation and tree growth over subtropical North America. *Paleoceanography and*  
866 *Paleoclimatology*, 34(5), 886–900. Article. <https://doi.org/10.1029/2018pa003510>
- 867 Torrence, C., & Compo, G. P. (1998). A practical guide to wavelet analysis. *Bulletin of the*  
868 *American Meteorological Society*, 79(1), 61–78. [https://doi.org/10.1175/1520-](https://doi.org/10.1175/1520-0477(1998)079<0061:APGTWA>2.0.CO;2)  
869 [0477\(1998\)079<0061:APGTWA>2.0.CO;2](https://doi.org/10.1175/1520-0477(1998)079<0061:APGTWA>2.0.CO;2)

- 870 Trouet, V., & Van Oldenborgh, G. J. (2013). KNMI Climate Explorer: A web-based research tool  
871 for high-resolution paleoclimatology. *Tree-Ring Research*, 69(1), 3–13.  
872 <https://doi.org/10.3959/1536-1098-69.1.3>
- 873 Vines, M., Tootle, G., Terry, L., Elliott, E., Corbin, J., Harley, G. L., et al. (2021). A paleo  
874 perspective of Alabama and Florida (USA) interstate streamflow. *Water*, 13(5), 657–668.  
875 <https://doi.org/10.3390/w13050657>
- 876 Volk, M. I., Hctor, T. S., Nettles, B. B., Hilsenbeck, R., Putz, F. E., & Oetting, J. (2017). Florida  
877 Land Use and Land Cover Change in the Past 100 Years. In E. P. Chassignet, J. W. Jones,  
878 V. Misra, & J. Obeysekera (Eds.), *Florida's climate: Changes, variations, & impacts* (pp.  
879 51–82). Gainesville, Florida: Florida Climate Institute.
- 880 Wigley, T. M. L., Briffa, K. R., & Jones, P. D. (1984). On the average value of correlated time  
881 series, with applications in dendroclimatology and hydrometeorology. *Journal of Climate*  
882 *and Applied Meteorology*, 23(2), 201–213. [https://doi.org/10.1175/1520-  
883 0450\(1984\)023<0201:OTAVOC>2.0.CO;2](https://doi.org/10.1175/1520-0450(1984)023<0201:OTAVOC>2.0.CO;2)
- 884 Wise, E. K., & Dannenberg, M. P. (2019). Climate factors leading to asymmetric extreme capture  
885 in the tree-ring record. *Geophysical Research Letters*, 46(6), 3408–3416.  
886 <https://doi.org/10.1029/2019gl082295>
- 887 Yeh, S. W., & Kirtman, B. P. (2005). Pacific decadal variability and decadal ENSO amplitude  
888 modulation. *Geophysical Research Letters*, 32(5). <https://doi.org/10.1029/2004GL021731>
- 889 Zang, C., & Biondi, F. (2015). treeclim: an R package for the numerical calibration of proxy-  
890 climate relationships. *Ecography*, 38(4), 431–436. <https://doi.org/10.1111/ecog.01335>

1     **Five Centuries of Groundwater Elevations Provide Evidence of Shifting Climate**  
2     **Drivers and Human Influences on Water Resources in North Central Florida**

3  
4     **Evan R. Larson<sup>1</sup>, Tom Mirti<sup>2\*</sup>, Thomas Wilding<sup>1†</sup>, and Chris A. Underwood<sup>1</sup>**

5     <sup>1</sup>Department of Environmental Sciences & Society, University of Wisconsin-Platteville

6     <sup>2</sup> Suwannee River Water Management District, Live Oak, Florida

7  
8     Corresponding author: Evan Larson (larsonev@uwplatt.edu)

9     \* Current affiliation: Retired; †Current affiliation: Nicolet Area Technical College

10  
11     **Key Points:**

- 12     • A 517-yr reconstruction of groundwater elevation indicates recent lows in North Central  
13     Florida approached megadrought conditions
- 14     • These extreme low groundwater elevations were likely caused in part by climate drivers  
15     and amplified by groundwater extraction
- 16     • Coupled oceanic-atmospheric phenomena drive variability in the persistence of  
17     groundwater elevations in North Central Florida

18 **Abstract**

19 Groundwater depletion is a concern around the world with implications for food security,  
20 ecological resilience, and human conflict. Long-term perspectives provided by tree ring-based  
21 reconstructions can improve understanding of factors driving variability in groundwater  
22 elevations, but such reconstructions are rare to date. Here, we report a set of new 546-year tree-  
23 ring chronologies developed from living and remnant longleaf pine (*Pinus palustris*) trees that,  
24 when combined with existing bald cypress (*Taxodium distichum*) tree-ring chronologies, were  
25 used to create a set of nested reconstructions of mean annual groundwater elevation for North  
26 Central Florida that together explain 63% of the variance in instrumental measurements and span  
27 1498–2015. Split calibration confirms the skill of the reconstructions, but coefficient of  
28 efficiency metrics and significant autocorrelation in the regression residuals indicate a  
29 weakening relationship between tree growth and groundwater elevation over recent decades.  
30 Comparison to data from a nearby groundwater well suggests extraction of groundwater is likely  
31 contributing to this weakening signal. Periodicity within the reconstruction and comparison with  
32 global sea surface temperatures highlight the role of El Niño-Southern Oscillation (ENSO) in  
33 driving groundwater elevations, but the strength of this role varies substantially over time.  
34 Atlantic and Pacific sea surface temperatures modulate ENSO influences, and comparisons to  
35 multiple proxy-based reconstructions indicate an inconsistent and weaker influence of ENSO  
36 prior to the 1800s. Our results highlight the dynamic influence of ocean-atmospheric phenomena  
37 on groundwater resources in North Central Florida and build on instrumental records to better  
38 depict the long-term range of groundwater elevations.

39

40

41 **Plain Language Summary**

42 Groundwater is an important source of freshwater for municipal and agricultural uses around the  
43 world. One major challenge to ensuring groundwater use is sustainable is that long-term records  
44 of its availability are scarce. This means we do not fully understand all the factors that influence  
45 groundwater availability or how groundwater resources may change in the future. One way to  
46 expand perspectives on groundwater resources is to use proxies, such as tree rings, to estimate  
47 past environmental conditions. Our team gathered tree-ring samples from old-growth longleaf  
48 pine trees in North Central Florida to develop a record of tree growth that spanned 546 years,  
49 from 1472–2018. Climate conditions that influenced tree growth at our site also influenced  
50 groundwater elevation. Based on this relationship, we reconstructed over five centuries of  
51 groundwater elevation changes. From this reconstruction, we now know that while deeper and  
52 more prolonged droughts than anything experienced during the instrumental record occurred in  
53 the past, the combined influences of climate and groundwater extraction drove recent  
54 groundwater elevations to lows comparable to some of the worst droughts in the past 500 years.  
55 As population continues to grow in Florida, residents and water managers can expect to face  
56 more extremes in groundwater elevations.

57

58

## 59 **1 Introduction**

60 Groundwater depletion is a significant concern in many regions of the world with critical  
61 implications for food security, ecological systems, and human conflict (Bierkens & Wada, 2019;  
62 Jasechko & Perrone, 2021). In the United States, declining groundwater levels documented  
63 across several broad areas raise concerns about the impacts of extraction and overexploitation on  
64 groundwater resources at regional scales (Jasechko & Perrone, 2021). For example, groundwater  
65 elevations in parts of the southeastern United States have declined over recent decades (Sutton et  
66 al., 2021), despite instrumental and tree-ring based perspectives indicating relatively wet  
67 conditions compared to recent decades and even centuries (Pederson et al., 2012). These  
68 contrasting patterns suggest that groundwater extraction for municipal and agricultural uses is  
69 outpacing recharge rates (e.g., de Graaf et al., 2019); however, in most cases instrumental  
70 records of groundwater are too short to clearly disentangle the effects of climate variability and  
71 extraction on groundwater elevations.

72

73 The longer-term perspectives enabled by proxy-based reconstructions would be immensely  
74 useful in considering changing groundwater conditions, but groundwater elevation is a  
75 challenging target to reconstruct. First, most time series of groundwater elevations are relatively  
76 short and many include numerous gaps from missing observations. This poses a challenge for  
77 robust calibration and verification (Fritts, 1976), particularly given the long-term persistence in  
78 groundwater systems relative to other aspects of climate such as precipitation (Sutton et al.,  
79 2021). Second, spatial variability in recharge mechanisms and the climate sensitivity of  
80 groundwater systems may differ from the available proxies, particularly trees whose growth is  
81 linked to atmospheric and surface conditions (Hunter et al., 2020). Third, widespread

82 groundwater extraction for agricultural and municipal purposes is altering groundwater levels  
83 around the world (Bierkens & Wada, 2019), potentially introducing trends in groundwater levels  
84 that are unrelated to atmospheric conditions that would otherwise link patterns in tree growth to  
85 changes in groundwater levels (Ferguson & St. George, 2003). Despite these challenges, the  
86 potential value of expanding perspectives on groundwater variability over multiple centuries to  
87 better understand their human and climatic drivers is immense and worth pursuing (Gholami et  
88 al., 2017), particularly where oceanic-atmospheric phenomena influence hydrologic conditions  
89 on time scales beyond the instrumental record (Gordu & Nachabe, 2021). This is the case in the  
90 southeastern United States, where growing populations are increasing demands on groundwater  
91 resources in a region where global sea surface temperatures strongly influence hydrologic  
92 conditions (Enfield et al., 2001; Schmidt et al., 2001).

93  
94 Among southeastern U.S. aquifers, the Floridian Aquifer System (FAS) covers approximately  
95 100,000 square miles and is the primary source of drinking water for millions of residents in  
96 Florida and Georgia (Miller, 1990). Well data across the FAS show increasing extraction and a  
97 decline in elevation of about 0.1–0.15 meter per year since 1950 (Barlow, 2003; Marella &  
98 Berndt, 2005). Cones of depression have formed around major cities within the FAS, such as  
99 Jacksonville, Florida, and in some cases local potentiometric gradients have reversed over  
100 instrumental records, creating the potential for encroachment of saltwater from coastal regions or  
101 from deep parts of the aquifer that contain saltwater (Miller, 1990). The installation of high-  
102 capacity wells to provide irrigation on sandy sites has also increased groundwater extraction in  
103 more rural areas (Marella & Berndt, 2005). Concerns over these groundwater impacts have been  
104 amplified by growing populations and increased demand for water. In northern Florida alone,

105 population increased by nearly 1 million residents since the early 2000s, placing considerable  
106 new demand on water resources (BEBR, 2011, 2020). With a growing population in the region  
107 and a diminishing groundwater supply, water resource managers in the Southeastern United  
108 States could benefit from the long-term perspective on water resource variability offered by  
109 dendrochronology.

110

111 Here, we report a set of new 546-year tree-ring chronologies developed from the rings of living  
112 and remnant old growth longleaf pine (*Pinus palustris*) in North Central Florida that, when  
113 combined with existing tree-ring chronologies developed from bald cypress (*Taxodium*  
114 *distichum*), enable the first annually resolved, multi-century reconstruction of groundwater  
115 elevation for the state. The resulting reconstruction extends records of groundwater by over 450  
116 years, provides a long-term perspective on shifting climate influences on groundwater elevation,  
117 and enables contextualization of recent declines in groundwater elevations for the region that are  
118 unprecedented in the historical record.

119

## 120 **2 Methods and Results**

### 121 2.1 Study area and field methods

122 Our study area is located in Goethe State Forest (GSF), a forest reserve in close proximity to  
123 three of Florida's five water management districts: the Suwannee River Water Management  
124 District (SRWMD), the St. Johns River Water Management District, and the Southwest Florida  
125 Water Management District (Figure 1a). These districts collectively encompass over 7.75 million  
126 hectares and are responsible for water supply planning for approximately 10 million people. The

127 landscape is relatively flat with low relief. Soils are sandy and extremely well drained, with  
128 subtle changes in topography creating substantial differences in plant communities. Current  
129 vegetation includes open stands of longleaf and slash pine (*Pinus elliottii*) with a saw palmetto  
130 (*Serenoa repens*) understory in upland settings, while relief of only 1–2 m results in marshes and  
131 wetlands dominated by slash pine and bald cypress (Figure 1b, 1c). The forest is managed for  
132 timber production, restoration of wire grass (*Aristida stricta*) plant communities, and red  
133 cockaded woodpecker (*Picoides borealis*) habitat. Mechanical thinning between 2000–2007 and  
134 widespread use of prescribed fire has been used to maintain an open savanna structure. During  
135 this period of intensive management, numerous old-growth longleaf pines were identified, along  
136 with an abundance of remnant stumps from logging *ca.* 1850 (Outland III, 2004).

137

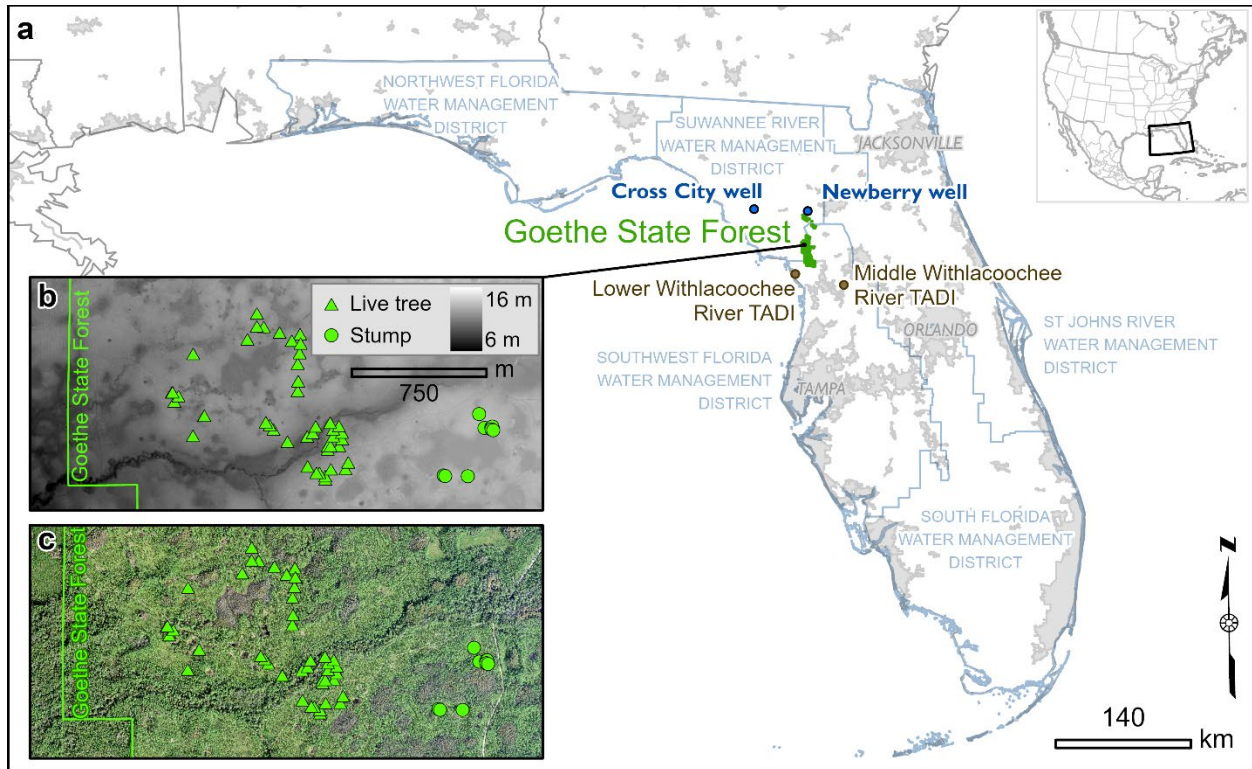
138 Groundwater elevation data are available from a network of monitoring wells that generally span  
139 the last several decades, however missing or discontinuous observations are common among  
140 these datasets. We screened numerous well logs from across the region and included two in the  
141 analyses presented here. First, the USGS Newberry well (S101722101) is the nearest long-term  
142 well to Goethe State Forest, one of the longest and most complete records investigated, and  
143 represents a continuous set of monthly observations from 1959–2020 (SRWMD, 2020). The  
144 second well considered here is the Cross City well (S101210001) which spans 1958–2020 but is  
145 more distant from the study site and includes 164 missing monthly observations, most of which  
146 occur from 1963–1979 (SRWMD, 2020). The value of the Cross City well is that it is farther  
147 from areas of intense groundwater use and should therefore represent past groundwater elevation  
148 most strongly influenced by climatic drivers rather than land use. For both wells, we calculated

149 average annual groundwater elevation from all available observations per year. The years 1974  
 150 and 1975 present gaps in the Cross City well time series where no observations were taken.

151

152

153



154

155 **Figure 1.** The study area in North Central Florida. (a) The location of Goethe State Forest  
 156 relative to the two wells used in this study, Florida water management district boundaries, and  
 157 major metropolitan areas, (b) a subset of the study area shown with a LiDAR-based DEM to  
 158 illustrate the distribution of sampled longleaf pine (*Pinus palustris*) trees and stumps relative to  
 159 subtle variations in topography, and (c) the same extent shown with color aerial imagery to  
 160 illustrate vegetation patterns created by topography.

161

162 Preliminary work in 2003 produced tree-ring chronologies from living old-growth longleaf pine  
163 and identified links between tree growth and hydrologic conditions in North Central Florida  
164 (Crockett et al., 2010). Additional sampling of both living trees and a small number of remnant  
165 stumps in 2008 produced a 438-yr chronology with significant climate information that provided  
166 important contributions to a reconstruction of the Suwannee River (Harley et al., 2017), but low  
167 sample depth in the mid-1800s coupled with a period of suppressed growth, both likely related to  
168 logging and resin extraction for the naval stores industry (Outland III, 2004), highlighted the  
169 need for additional sampling. A third phase of sampling in 2017 and 2019 specifically targeted  
170 living trees to update the existing chronologies and additional remnant longleaf pine stumps to  
171 extend the chronology further into the past, increase sample depth in the overlap between living  
172 trees and remnant stumps, and enhance signal strength during the 1800s.

173  
174 Sampling focused on living trees that visually exhibited old-growth characteristics, including the  
175 presence of robust limbs in the canopy, flattened canopy structure, absence of lower limb stubs,  
176 acute distortion of sub-canopy limbs, and the presence of peel scars associated with turpentine  
177 production, which ended around 70 years ago in northern Florida (Figure 2a, 2b). Increment core  
178 samples were collected along 1–4 radial transects of each living tree, with the number of  
179 transects determined by the shape, size, and symmetry of the tree. Stumps were initially sampled  
180 opportunistically until their value became more evident. Later, to improve the efficacy of  
181 targeted stump sampling, the study area was scouted following winter prescribed fires that  
182 reduced ground cover and maximized the likelihood of locating low-profile stumps. Stump  
183 sampling specifically targeted specimens that exhibited deep weathering, char, and evidence of  
184 box-cuts associated with resin collection activities in the 1800s. All sampled stumps were cut

185 with a chainsaw as low to the ground as possible to ensure collection of the maximum number of  
186 growth rings, with later recognition that ground-level samples also enhanced the potential for  
187 their use in fire history research (Huffman & Rother, 2017). A visual chronosequence emerged,  
188 with different types of cambial scars associated with different periods of turpentine harvesting  
189 techniques and the oldest samples coming from snags that were likely from trees that died prior  
190 to 1800s logging and turpentine activities (Figure 2b, 2c, 2d).

191



192

193 **Figure 2.** Site and tree characteristics used to guide sample collection. (a) Open stand structure  
194 has been maintained through mechanical treatments and prescribed burns, with old growth  
195 longleaf pine retained to provide habitat for the endangered red cockaded woodpecker (indicated  
196 by white band on the tree at far right). Relative sample age was estimated by (b) living trees with  
197 “catface” scars associated with turpentine activities in the late 1800s and early 1900s, (c) box  
198 cuts associated with turpentine activity in the middle to late 1800s, and (d) remnant snags with  
199 no evidence of turpentine collection from trees that likely died prior to logging or the  
200 establishment of industrial turpentine activities on site.

## 201 2.2 Tree Ring Chronology Development

202 Cross sections were frozen at *ca.*  $-20^{\circ}\text{C}$  for at least 24 hours prior to sanding to reduce the  
203 emergence of resin during the finishing process, then surfaced using hand-held belt sanders and  
204 progressing from ANSI 40-grit to ANSI 400-grit. Pneumatic palm sanders with microfinishing  
205 film were then used to maintain cool temperatures while progressively sanding to a final grit of  
206 20-micron sanding discs. Each sample was polished with steel wool to achieve the final surface.  
207 A similar progression of sanding was applied to core samples, but by hand-sanding.

208

209 Two to four paths were identified on each cross section, depending on the shape and condition of  
210 the sample, while a single transect was identified on each core sample. The annual rings of each  
211 sample were identified under  $4.5\text{--}40\times$  magnification and internally crossdated to account for  
212 locally-absent growth rings and intra-annual variations in wood density, commonly referred to as  
213 false rings. Each path was scanned at 1800 dpi optical resolution using an Epson 10000XL  
214 flatbed scanner. The images of each path were imported to WinDENDRO v2014 and measured  
215 for total ring width (TRW), earlywood width (EW), and latewood width (LW). The boundary  
216 between earlywood and latewood growth was determined as the first formation of latewood cells  
217 within each ring and a regression-based latewood measurement series ( $LW_{\text{reg}}$ ) was created for  
218 each path by removing the shared variability between earlywood and latewood widths through  
219 linear regression (*sensu* Griffin et al., 2011).

220

221 Crossdating was strong within the final longleaf pine tree-ring data set, with a total of 172 dated  
222 measurement series from 91 trees, of which 59 were living and 32 were remnants. The data set  
223 spanned the years 1472–2018 and exhibited an expressed population signal of  $>0.85$  from 1505–

224 2018 (Figure 3a, 3b). Visual inspection of the raw longleaf pine ring width data indicated a  
225 distinct decade or more of suppressed growth from the late 1800s to the early 1900s, likely the  
226 result of extensive cambial damage from turpentine activities, followed by growth releases  
227 (Figure 3a). We emphasized the variability likely related to interannual climate variations despite  
228 these releases and suppressions in tree growth by normalizing each ring-width measurement  
229 series using a power transformation method described by Cook and Peters (1997). The  
230 normalized measurement series were then used to develop a total of 16 versions of standardized  
231 ring width-index (RWI) chronologies from the longleaf pine, as described below.

232  
233 First, two versions of standard (STD) chronologies were created for each type of measurement  
234 collected from the longleaf pine (TRW, EW, LW, and  $LW_{reg}$ ). Each normalized measurement  
235 series was fit with a spline of 50% frequency cutoff at a 30-year frequency to remove low-  
236 frequency variability from the ring width series (Cook & Peters, 1981). The values from each  
237 resulting ring-width index series were then used to calculate an annually-resolved RWI  
238 chronology using a robust bi-weight mean (Cook, 1985). This resulted in chronologies with  
239 minimal evidence of the disturbance effects (GSF30; Figure 3b). Second, each normalized  
240 measurement series was fit using a stiffer spline with 50% frequency cutoff at the 100-year  
241 frequency to retain a greater proportion of the low-frequency variability within the ring-width  
242 series, and again combined into RWI chronologies using bi-weight means of annual values. The  
243 resulting chronologies retained more information that could provide insight to the low-frequency  
244 variability of hydrologic conditions in Florida, but also retained more evidence of the growth  
245 suppression (GSF100; Figure 3b). This produced eight STD chronologies, including TRW, EW,  
246 LW, and  $LW_{reg}$  based on both the GSF30 and GSF100 standardization approaches.

247  
248 Second, an additional eight residual (RES) chronologies were created by applying the same  
249 standardization methods described above (GSF30 and GSF100), but fitting each of the individual  
250 ring width index series to an Autoregressive-Moving-Average Model before combining the  
251 resulting annual values using a robust bi-weight mean (Meko, 1981). The RES chronologies  
252 therefore expressed less autocorrelation and better emphasized inter-annual variations of tree  
253 growth than the STD chronologies. In all, this resulted in a total of sixteen standardized tree-ring  
254 chronologies from the longleaf pine measurements: standard (STD) and residual (RES)  
255 chronologies based on TRW, EW, LW, and  $LW_{reg}$ , with two versions of each chronology based  
256 on standardization with 30-year smoothing splines (GSF30) and 100-year smoothing splines  
257 described above (GSF100).

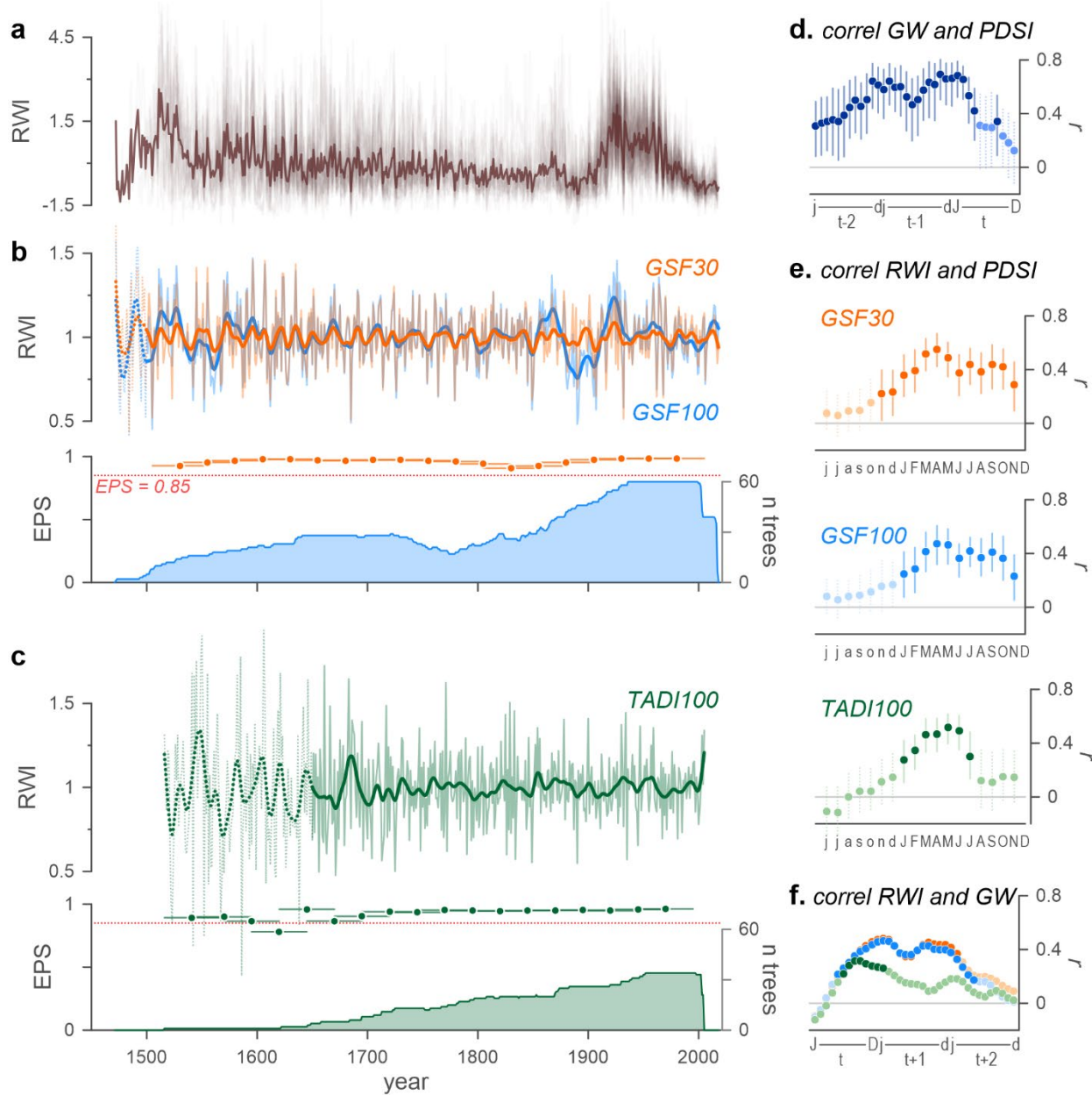
258  
259 In addition to the newly developed longleaf pine chronologies, tree-ring width data from  
260 previously developed bald cypress trees (*Taxodium distichum*) growing at two nearby sites along  
261 the Withlacoochee River were collected from the International Tree-Ring Databank (Carr &  
262 Stahle, 2010; D. W. Stahle et al., 2010) (Figure 1). The bald cypress data included earlywood,  
263 latewood, and total ring width measurements, and we calculated a  $LW_{reg}$  series for each  
264 measurement series following the same methods as used for the longleaf pine (Griffin et al.,  
265 2011). Initial analyses indicated a common signal shared by the bald cypress trees from the two  
266 sites, which were therefore combined into a single set of measurement series for chronology  
267 development. In all, the bald cypress ring-width data included 74 measurement series from 34  
268 trees and spanned 1516–2005, with an  $EPS > 0.85$  from 1650–2005 (Figure 3c). The bald cypress  
269 ring-width data exhibited few synchronous disturbance events and were therefore standardized to

270 develop eight total chronologies—four STD created using splines of 50% frequency cutoff at  
271 100-year frequency to retain low-frequency growth patterns that could be linked to multi-decadal  
272 climate variability and four RES chronologies (TADI100; Figure 3c).

273

274 The complete set of chronologies included 16 longleaf pine chronologies and 8 bald cypress  
275 chronologies, each of which were clipped to the first year of a 50-yr window where the  
276 expressed population signal was  $>0.85$  (Wigley et al., 1984) to ensure a robust signal for climate  
277 and growth analyses (Figure 3b, 3c). The standardization process was carried out using the  
278 computer program Arstan v44xp (Cook & Krusic, 2013).

279



280

281 **Figure 3.** Linking tree growth to groundwater elevation. (a) Raw ring-width measurements of  
 282 the 172 ring-width series from 91 longleaf pine trees and stumps sampled at Goethe State Forest,  
 283 here normalized to a series mean of 0 with the sample-set mean shown in dark brown to illustrate  
 284 a deep suppression that spanned the 1890s into the early 1900s that was followed by a sharp  
 285 growth release that together likely represent land use changes associated with logging and  
 286 turpentine operations at the site. (b) Two sets of standardized ring width-index chronologies for

287 the longleaf pine, here developed from total ring width, shown to illustrate the influence of land  
288 use on tree growth and how the applied standardization methods (GSF30 with its 30-year  
289 smoothing splines depicted in orange vs. GSF100 with its 100-year smoothing splines depicted  
290 in blue) retained more or less low-frequency information in the resulting chronologies;  
291 interannual chronology values are shown as thin lines with the chronologies smoothed using 15-  
292 year splines shown as bold; sample depth and expressed population signals indicate both  
293 chronologies are robust from 1505–2018 ( $EPS > 0.85$  where chronology lines are solid). (c) The  
294 standardized ring-width index chronology derived from bald cypress trees growing along the  
295 nearby Withlacoochee River (TADI100; green) shown as annual values (thin line) and smoothed  
296 with a 15-yr spline (bold line), EPS ( $EPS > 0.85$  where chronology lines are solid), and sample  
297 depth. (d) Correlation coefficients (symbol) and confidence intervals (whiskers) between mean  
298 annual groundwater elevation and monthly PDSI, from year  $t-2$  to  $t$ , with bold colors indicating  
299 significant correlations ( $p < 0.05$ ). (e) Correlation coefficients and confidence intervals between  
300 each RWI chronology and monthly PDSI over the instrumental period, spanning from the  
301 previous year (lower case) to the current year (upper case), with bold colors indicating  
302 significant correlations ( $p < 0.05$ ). (f) Correlation coefficients between each of the total ring width  
303 RWI chronologies and mean monthly groundwater elevation over three years, from  $t$  to  $t+2$ , with  
304 bold colors indicating significant correlations ( $p < 0.05$ ).

305

## 306 2.4 Calibration, Verification, and Climate Reconstructions

307 Longleaf pine in this region of Florida are particularly sensitive to changes in hydrology because  
308 of the low water holding capacity of the sandy soils common to the region. Slight changes in  
309 depth to groundwater in such soils can have substantial effects on tree access to moisture

310 (Ciruzzi & Loheide, 2021; Foster & Brooks, 2001). Where access to groundwater does not  
311 directly impact tree growth, similar responses to precipitation and moisture balances may enable  
312 the identification of robust linkages between tree growth and groundwater elevation (Perez-  
313 Valdivia & Sauchyn, 2011). We therefore approached calibration of our tree-ring and  
314 groundwater data through a stepwise process that examined the environmental variables that  
315 could mechanistically link variability in tree growth and groundwater elevation. The  
316 relationships among these data were examined using correlation analyses as implemented in the  
317 `dcc()` function of the `treeClim` package of R (Zang & Biondi, 2015).

318  
319 First, we compared the relationships among instrumental climate data and groundwater  
320 variability through correlation analysis of both monthly and seasonal variables. The data used in  
321 this analysis included monthly precipitation, maximum temperature, and Palmer's Drought  
322 Severity Index (PDSI) time series from 1895–2017 for NCDC Florida Division 3 (NCDC, 2018),  
323 and groundwater elevation above the National Geodetic Vertical Datum of 1929 measured on the  
324 27th of each month near Newberry, Florida, at well S101722001 from 1959–2018 (Figure 1)  
325 (SRWMD, 2020). The USGS Newberry well was selected for its proximity to the study area and  
326 for the complete record it provided. The relationships among these data were examined for  
327 current and lagged relationships of up to two years using correlation analyses to identify links  
328 between atmospheric conditions and groundwater elevation. The strongest identified relationship  
329 between climate variables and groundwater elevation included a significant correlation between  
330 PDSI and groundwater elevation at up to a two-year lag, indicating persistence in the  
331 groundwater system (Figure 3d).

332

333 The climate responses of the 16 longleaf pine chronologies and 8 bald cypress chronologies  
334 exhibited similar overall relationships between tree growth and climate, with positive  
335 correlations to precipitation and PDSI and inverse relationships with maximum temperatures,  
336 though these varied by species and by the portion of the growth ring on which the chronologies  
337 were based (Figure S1). Differences in the seasonal timing of climate response were evident  
338 between EW and LW chronologies, and the window of climate response was narrower among  
339 the bald cypress chronologies than the longleaf pine chronologies (Figure S1). The strongest  
340 climate-growth relationships among all chronologies were consistently associated with PDSI  
341 (Figure 3e). This result supported the notion that soil moisture availability, as represented by  
342 PDSI, was directly related to both groundwater elevation and tree growth. Direct comparison of  
343 groundwater elevation and the tree-ring chronologies identified significant correlations that  
344 spanned windows of 8–25 months, with the strongest and most temporally expansive  
345 relationships identified with the longleaf pine chronologies (Figure 3f, Figure S2).

346

347 Based on the observed relationships among climate, tree growth, and groundwater, we created a  
348 final set of predictors for a regression-based reconstruction by identifying the common variance  
349 among those tree-ring chronologies that showed significant correlations to groundwater  
350 elevation. First, all chronologies were clipped to include only the period where subsample  
351 strength was  $>0.85$ , indicating a robust signal suitable for reconstruction (Buras, 2017). We then  
352 assembled two separate matrices of tree-ring chronologies, one based on the GSF30 and  
353 TADI100 chronologies and one based only on the GSF100 chronologies. Persistence in the  
354 groundwater system that created lagged climate-groundwater relationships (Figure 3d) and tree  
355 physiology that resulted in lagged climate-growth relationships (Figure 3e) were accounted for

356 by lagging the chronologies in each matrix from  $t-4$  to  $t+4$ . The matrices were then refined by  
357 correlating each version of the chronologies with annual groundwater elevation at the USGS  
358 Newberry Well and retaining only those that exhibited significant Pearson product moment  
359 correlations ( $p < 0.01$ ). The first matrix spanned 1695–2002 and included 10 chronologies, five  
360 from the GSF30 and four from the TADI100 data sets. The second matrix spanned 1498–2015  
361 and included nine chronologies from the GSF100 data. We reduced the multicollinearity in each  
362 matrix using principle components analysis (PCA) as implemented by the `prcomp()` function in  
363 R (R Development Core Team, 2019).

364  
365 The principle components (PCs) derived for each matrix were considered in the development of  
366 two linear regression models using a forward and backward selection stepwise procedure as  
367 implemented in the `step()` function of R (R Development Core Team, 2019). The resulting  
368 reconstructions were assessed through a split calibration and verification process on the early and  
369 late halves of each calibration period using the `skill()` function in the R package `treeClim` (Zang  
370 & Biondi, 2015), rescaled to the instrumental record, and examined for potential bias using an  
371 extreme value capture test (McCarroll et al., 2015).

372  
373 The final GSF100 regression model explained 60% of the variance in mean annual instrumental  
374 groundwater elevation at the Newberry Well from 1959–2015, and the GSF30+TADI100  
375 reconstruction explained 60% of the variance in instrumental annual groundwater elevation from  
376 1959–2002 (Figure 4a). Both reconstructions were skillful, with reduction of error statistics of  
377 0.62–0.69 (Table 1). The coefficient of efficiency (CE) was positive in all cases, though it was  
378 close to zero when calibrated on the early split of the GSF100 reconstruction (Table 1). Of note,

379 when calibration and verification of the GSF100 reconstruction were conducted over the same  
380 period as the GSF30+TADI100 reconstruction (1959–2002), CE was strongly positive for both  
381 splits (see  $GSF100_{\text{trim}}$  in Table 1). Durbin-Watson  $d$  statistics were significant for all but the  
382 GSF100 late split based on the shortened calibration window which indicated significant  
383 autocorrelation in the model residuals. Visual inspection of the model showed the tree-ring  
384 reconstructions over-estimated groundwater elevation in more recent decades (Figure 4a).  
385 Comparing first-difference time series of both the instrumental and reconstructed time series  
386 indicated significant predictive power in the reconstructions even when trend was removed  
387 (Figure 4a). These results collectively indicate that useful information is provided by these  
388 reconstructions and also suggest the influence of a driving factor that affected groundwater  
389 elevation but not tree growth over the most recent decades.

390  
391 The two reconstructions were complementary. The reconstruction based on the  
392 GSF30+TADI100 chronologies did not extend as far into the past or as close to the present but  
393 retained low frequency variability most likely related to climate from the TADI100 chronologies,  
394 while the GSF30 chronologies contributed information about high-frequency variability with  
395 minimal influence of the late 1800s turpentine industry/land use signal (Figure 4b). The  
396 reconstruction based on the GSF100 chronologies extended further into the past and closer to the  
397 present, but due to the more conservative standardization retained low frequency variability in  
398 the late 1800s and early 1900s that represented land use influences and not climatic information  
399 (Figure 4b). Analysis of the extreme value capture (McCarroll et al., 2015) indicated that both  
400 the GSF30+TADI100 and the GSF100 reconstructions exhibited biases toward better  
401 representation of extreme high groundwater elevation ( $EVC = 3/4$  and  $4/6$ , respectively, both  $p <$

402 0.01) as compared to extreme low elevation (EVC = 2/4 and 2/6). This wet-bias is unusual  
403 among tree-ring-based hydrologic reconstructions that often better represent dry conditions  
404 (Wise & Dannenberg, 2019). This result could be explained by the persistence in groundwater  
405 elevations, where the relatively open groundwater aquifer created by the extremely well-drained  
406 sandy soils of the site may smooth out the effects of short-duration, extreme rainfall events that  
407 are often missed by trees growing in arid conditions. Alternatively, the asymmetry could be  
408 explained by non-climatic factors. All of the groundwater elevations within the 10<sup>th</sup> lowest  
409 percentile in the instrumental record occurred since 2001, the period of greatest potential impacts  
410 from groundwater extraction. Extreme lows in groundwater elevation driven in part by human  
411 factors would be absent in tree-ring records that more purely express climate drivers. Regardless  
412 of the reasons behind the asymmetrical extreme capture characteristics of the chronologies, the  
413 overall similarity in response of the two chronologies supported creation of a spliced  
414 reconstruction by adding the early and late portions of the GSF100 reconstruction onto the  
415 GSF30+TADI100 reconstruction. The resulting spliced chronology explained 63% of the  
416 variance in mean annual instrumental groundwater elevation and retained low-frequency signal  
417 throughout while minimizing the potential influence of land use in the 1800s (Figure 4a, 4c).  
418

419 As a final assessment of the spliced reconstruction, we compared the spatial footprints of  
420 instrumental and reconstructed groundwater elevation responses to drought and sea surface  
421 temperatures using KNMI Climate Explorer (Trouet & Van Oldenborgh, 2013). Spatial  
422 correlations with drought showed responses centered on northern Florida (Figure 5a), while  
423 correlations with sea surface temperatures depicted a clear relationship with El Niño-Southern  
424 Oscillation variability over the instrumental period (Figure 5b). Although both spatial signatures

425 were somewhat weaker with the reconstruction than the instrumental data, the geographic extent  
 426 and strength of the correlations were generally similar, broadly supporting the skill of the  
 427 reconstruction (Tegel et al., 2020).

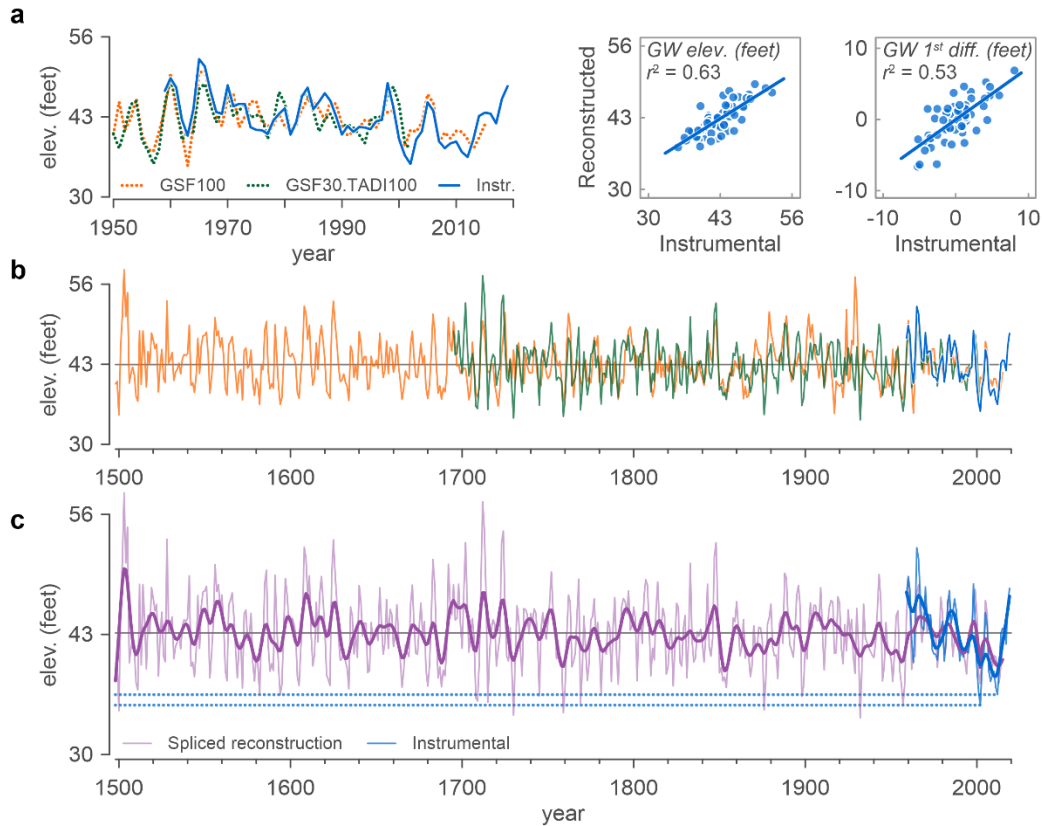
428

429 **Table 1.** Calibration and verification statistics for reconstructing mean annual groundwater  
 430 elevation in North Central Florida. The GSF100<sub>trim</sub> model results are based on the same  
 431 calibration window as the GSF30+TADI100 model. The spliced reconstruction includes the  
 432 GSF30+TADI100 model for years 1959–2002 and the GSF100 model for years 2003–2015.

Reconstruction	Calibration period	Validation period	$r^2$	RE	CE	$d$
GSF100	1959–2015		0.60			
	1959–1987	1988–2015	0.55	0.62	0.03	1.21*
	1988–2015	1959–1987	0.55	0.69	0.26	1.30*
GSF100 <sub>trim</sub>	1959–2002		0.57			
	1959–1980	1981–2002	0.57	0.61	0.26	1.04*
	1981–2002	1959–1980	0.61	0.53	0.52	1.71
GSF30+TADI100	1959–2002		0.60			
	1959–1980	1981–2002	0.64	0.62	0.45	0.99*
	1981–2002	1959–1980	0.50	0.69	0.56	0.90*
Spliced reconstruction	1959–2015		0.63			

433 \* indicates  $p < 0.05$

434



435

436 **Figure 4.** Calibration, verification, and reconstruction of mean annual groundwater elevation for

437 the Newberry USGS Well in North Central Florida. (a) Comparison of two versions of the

438 reconstruction (GSF100 only, GSF30+TADI100) with instrumental mean annual groundwater

439 elevation, along with scatter plots comparing the spliced reconstruction and instrumental

440 groundwater elevation. A similar scatter plot based on first-differenced versions of the

441 reconstruction and instrumental record is presented to specifically compare the high-frequency

442 patterns of the time series. (b) The full GSF100 and GSF30+TADI100 reconstructions along

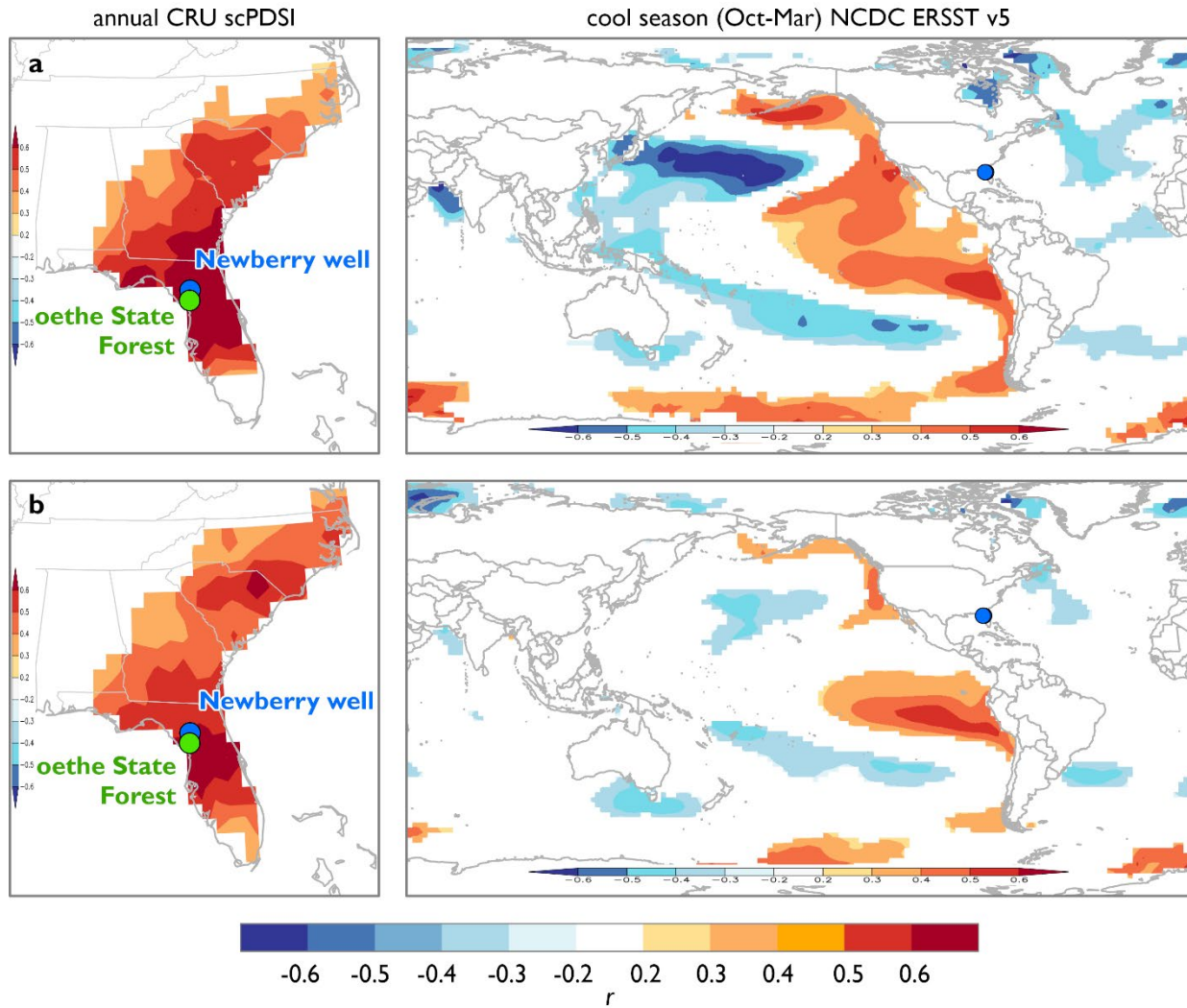
443 with the instrumental record. (c) The final spliced reconstruction shown relative to the

444 instrumental record, both with 15-yr smoothing splines to emphasize lower-frequency variations

445 in groundwater elevation. Thin horizontal dotted lines are included to compare extreme

446 individual-year lows in the instrumental record to the longer-term reconstruction.

447



448

449 **Figure 5.** Spatial climate response of instrumental and reconstructed groundwater elevation.

450 Correlation of (a) instrumental and (b) reconstructed annual groundwater elevation with drought

451 (scPDSI, 1959–2015) and sea surface temperatures (ERSST v5, 1977–2015). Correlations with

452 sea surface temperatures were stratified based on shifting relationships with ocean conditions

453 over time, as detailed below.

454

## 455 2.5 Interpreting the reconstruction: long-term variability in groundwater resources

456 The spliced reconstruction of mean annual groundwater elevation at the USGS Newberry well  
457 presented here extends information on groundwater elevation over 450 years beyond the  
458 instrumental record of the well, and over 400 years beyond any instrumental groundwater record  
459 in Florida. This expanded temporal perspective allows modern events to be viewed in the context  
460 of long-term variability; however, the calibration and verification results require additional  
461 consideration regarding the differing CE results for the GSF100 reconstruction when the most  
462 recent two decades are included in the calibration and the significant residuals in each version of  
463 the reconstruction. Comparing groundwater elevations recorded at the USGS Newberry well to  
464 those recorded at the Cross City well supports the notion that these results represent a dampening  
465 of the linkages that connect atmospheric conditions, tree rings, and groundwater elevations as the  
466 influences of groundwater extraction increase.

467

468 The Cross City well is located at the landward edge of Florida's Big Bend coastal zone, which,  
469 until somewhat recently, has been one of the least developed coastal regions of the United States  
470 (Volk et al., 2017). The Cross City well is thus more distant from urban centers and areas of  
471 intense agricultural groundwater use, making it less likely to be influenced by groundwater  
472 extraction (Figure 1), and while the numerous missing observations early in the record limit its  
473 usefulness as a target for calibration and reconstruction, the data do offer insight for interpreting  
474 the Newberry reconstruction. Comparing z scores for instrumental mean annual groundwater  
475 elevations at the Cross City and Newberry wells identifies an increasing difference between  
476 groundwater elevations at the two sites over time that is more pronounced during years of low  
477 groundwater (Figure 6a, 6b). This pattern matches both observed and modeled impacts of

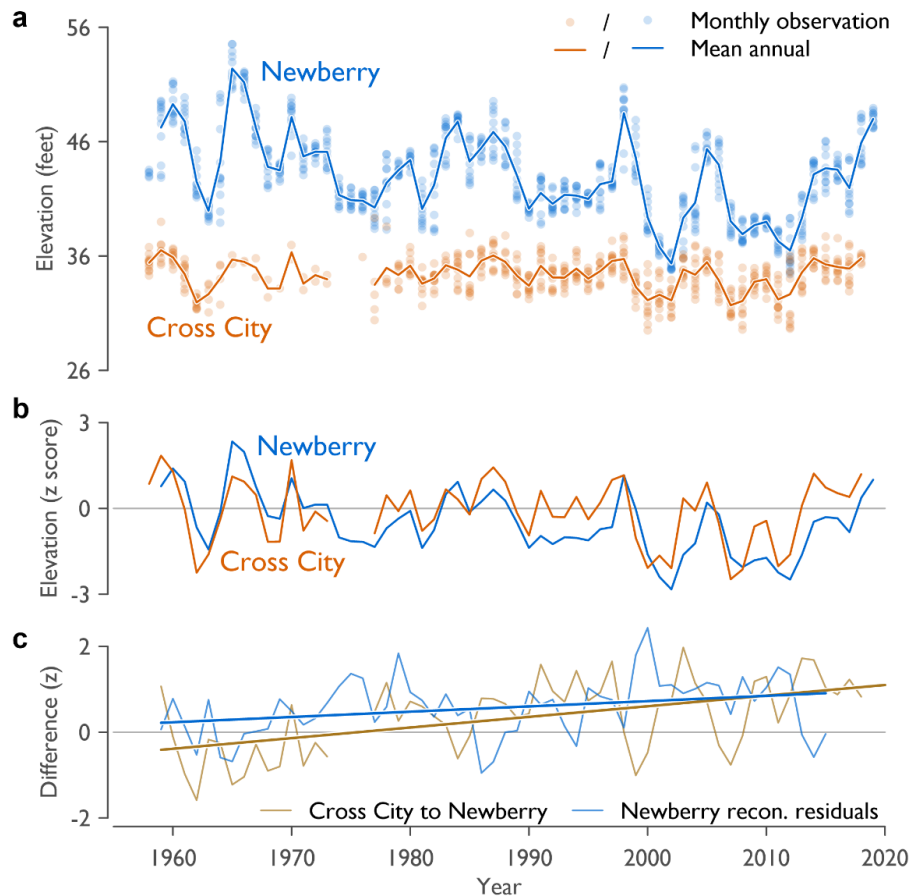
478 groundwater withdrawals on regional groundwater elevations (Gordu & Nachabe, 2021).  
479 Comparing the difference between the two well records to the Newberry reconstruction  
480 residuals, with both transformed into z scores, shows a similar increasing trend over time (Figure  
481 6c). Taken together, and in the context of known increases in groundwater extraction (Marella &  
482 Berndt, 2005), the increasing difference between groundwater elevation at the Cross City and  
483 USGS Newberry wells and the overestimation of recent groundwater elevation in the Newberry  
484 reconstruction represent a weakening of climatic control over groundwater elevation that is likely  
485 unprecedented. This also suggests that future low groundwater elevation will be amplified by  
486 groundwater extraction, increasing the probability of water resource scarcity beyond what has  
487 been experienced in at least the past 500 years.

488

489 The implications for interpreting the overall reconstruction are substantial, but do not undermine  
490 the value of the results reported here. Given the relatively recent development of high-capacity  
491 wells in the vicinity of the USGS Newberry well, and supported by data from modeling efforts, it  
492 is likely that substantial human impacts on groundwater elevation began in the 1990s and have  
493 increased since that time (Gordu & Nachabe, 2021). This means the calibration dataset provides  
494 at least three decades of relatively stable relationships among climate, groundwater elevation,  
495 and tree growth. The weakening of these relationships and amplified declines in groundwater  
496 elevation over recent decades, when included in the calibration and particularly when used to  
497 rescale the reconstruction, could bias the overall mean of the reconstruction. However, the strong  
498 relationship between the first-differenced instrumental and reconstructed time series and the  
499 similar spatial climate responses suggest that the reconstruction accurately captures interannual  
500 variability in groundwater elevation. Based on the assumption of stable climate-groundwater-tree

501 growth relationships prior to the period of groundwater extraction, we suggest that the  
 502 reconstruction presented here is a valid representation of pre-instrumental groundwater elevation.

503



504

505 **Figure 6.** Groundwater elevations at two wells in North Central Florida illustrate regionally  
 506 declining groundwater levels. (a) Observed mean annual groundwater elevations at the USGS  
 507 Newberry and Cross City wells. (b) Z scores of mean annual groundwater elevations for both  
 508 wells illustrating how the USGS Newberry instrumental measurements trend lower than those of  
 509 the Cross City well since ca. 1990. (c) Trend in the difference between instrumental groundwater  
 510 elevations at the Cross City well and the USGS Newberry well are similar to the Newberry  
 511 reconstruction residuals, reflecting the possible impacts of extraction on groundwater elevations  
 512 at the USGS Newberry well.

513 Given the considerations outlined above, the reconstruction of mean annual groundwater  
514 elevation at the USGS Newberry well provides important historical context for modern  
515 hydrologic conditions. First, as is the case with nearly all proxy-based hydrologic  
516 reconstructions, the distribution of reconstructed annual groundwater elevation for the  
517 instrumental period does not match the range of conditions represented over the full length of the  
518 reconstruction (Figure 7a). Reconstructed single year extreme lows and highs surpass the most  
519 extreme conditions observed since the start of direct groundwater elevation monitoring (Table 2)  
520 and suggest caution in basing long-term forecasts of water availability on the historical record  
521 (Pederson et al., 2012). Individual years and extended pluvial conditions in the mid-1500s, early  
522 1600s, and early 1700s exhibited higher groundwater elevations than experienced at any point in  
523 the instrumental period. At the same time, the low instrumental groundwater elevations recorded  
524 in 2002 and 2012 are among the lowest 5% of reconstructed groundwater elevations in the past  
525 500 years (Figure 4c, Table 2). The same years in the reconstruction are within the lowest 6%,  
526 and 15%, respectively—low, but not as extreme.

527

528 The more extreme ranking of these years based on instrumental records may be related to the  
529 extreme capture characteristics of the reconstruction, in that proxy-based records do not readily  
530 represent the most extreme conditions of the target variable (McCarroll et al., 2015). If that is the  
531 case, it would suggest that past lows in groundwater elevation in the reconstruction  
532 underestimate actual elevation and therefore serve as a conservative estimation of worst-case  
533 conditions. An alternative interpretation is that the reconstruction accurately represents the  
534 climatological influences on groundwater elevation and that groundwater extraction amplified  
535 these lows to extreme levels over recent decades. If true, this suggests that not only are the return

536 of extreme low groundwater conditions unavoidable due to climate variability, but that these  
537 conditions will be amplified by current and ongoing groundwater extraction. This increases the  
538 likelihood of North Central Florida experiencing more severe water deficits than experienced in  
539 the instrumental period thus far.

540

541 Building on the perspective gained from individual years, considering the consecutive number of  
542 years of above or below average groundwater elevation, or runs, provides a useful perspective on  
543 the duration of high- or low-groundwater conditions. We calculated runs relative to the mean of  
544 the full reconstruction ( $\bar{x} = 43.14$  feet above the National Geodetic Vertical Datum of 1929 from  
545 1498–2015) as a way to further place recent groundwater elevations in a long-term context  
546 (Figure 7b). The median run length was 2 years for both above- and below-average groundwater  
547 elevations, suggesting ground water elevations were primarily characterized by high-frequency  
548 variability; however, this was not consistent through time. Periods of more persistent above- and  
549 below-average conditions occurred at several points in the reconstruction, including from the  
550 mid-1500s through the early 1600s, and at approximately 50–70-year intervals from ca. 1700  
551 through 2000 (Figure 7b). The longest distinct run for above-average conditions relative to the  
552 long-term record was 10 years long and spanned 1791–1801, while the longest below-average  
553 runs included two 9-year periods of low groundwater from 1989–1997 and from 2007–2015.

554

555 Shifting levels of persistence in the reconstruction suggests shifting climate drivers of  
556 groundwater elevation. To supplement the runs analysis, we examined the power spectra of the  
557 reconstruction using a continuous Morlet wavelet transform calculated by the `morlet()` function  
558 in `dplr` (Bunn, 2008; Torrence & Compo, 1998). Significant periodicities at 5–15 years

559 identified throughout the 1500s into the early 1600s, again in the late 1600s into the mid-1700s,  
560 and sporadically throughout the 1800s and 1900s (Figure 7c) generally align with the periods of  
561 greater persistence identified in the runs analysis (Figure 7b). Significant periodicity in the ca.  
562 100-year band is evident from the 1600s through the 1900s and again aligns with peaks in  
563 persistence in the runs analysis centered on the years 1600, 1700, 1800, 1900, and possibly 2000.  
564 Interpretation of this response is problematic as frequencies above 100 years were largely  
565 removed from the tree-ring chronologies via standardization (Figure 7c). Collectively,  
566 interpretation of the runs and wavelet spectra suggest an important role in groundwater  
567 elevations for climate drivers that exhibit oscillatory behaviors, but that the influences of these  
568 factors wax and wane through time.

569  
570 The expression of shifting persistence in groundwater elevation variability is illustrated by  
571 considering cumulative anomalies, defined here as the sum of annual groundwater elevation  
572 anomalies over continuous periods of above- or below-average groundwater elevation relative to  
573 the reconstruction mean. Periods of low persistence such as those in the mid-1600s and early  
574 1800s generally aligned with near-average groundwater elevations, while periods of greater  
575 persistence coincided with deep pluvial or drought conditions (Figure 7d). For example,  
576 cumulative anomalies of below-average groundwater elevations clustered in the late 16<sup>th</sup> century,  
577 which is a period of megadrought documented across much of North America (David W. Stahle  
578 et al., 2007). In this context, recent cumulative anomalies of below-average groundwater  
579 elevations, driven in part by the rise in persistence over recent decades, were surpassed only once  
580 in the past 500 years (Figure 7c, 7d). Furthermore, the overestimation of groundwater elevation  
581 for recent decades of the reconstruction (Figure 6) suggests that while hydrologic drought

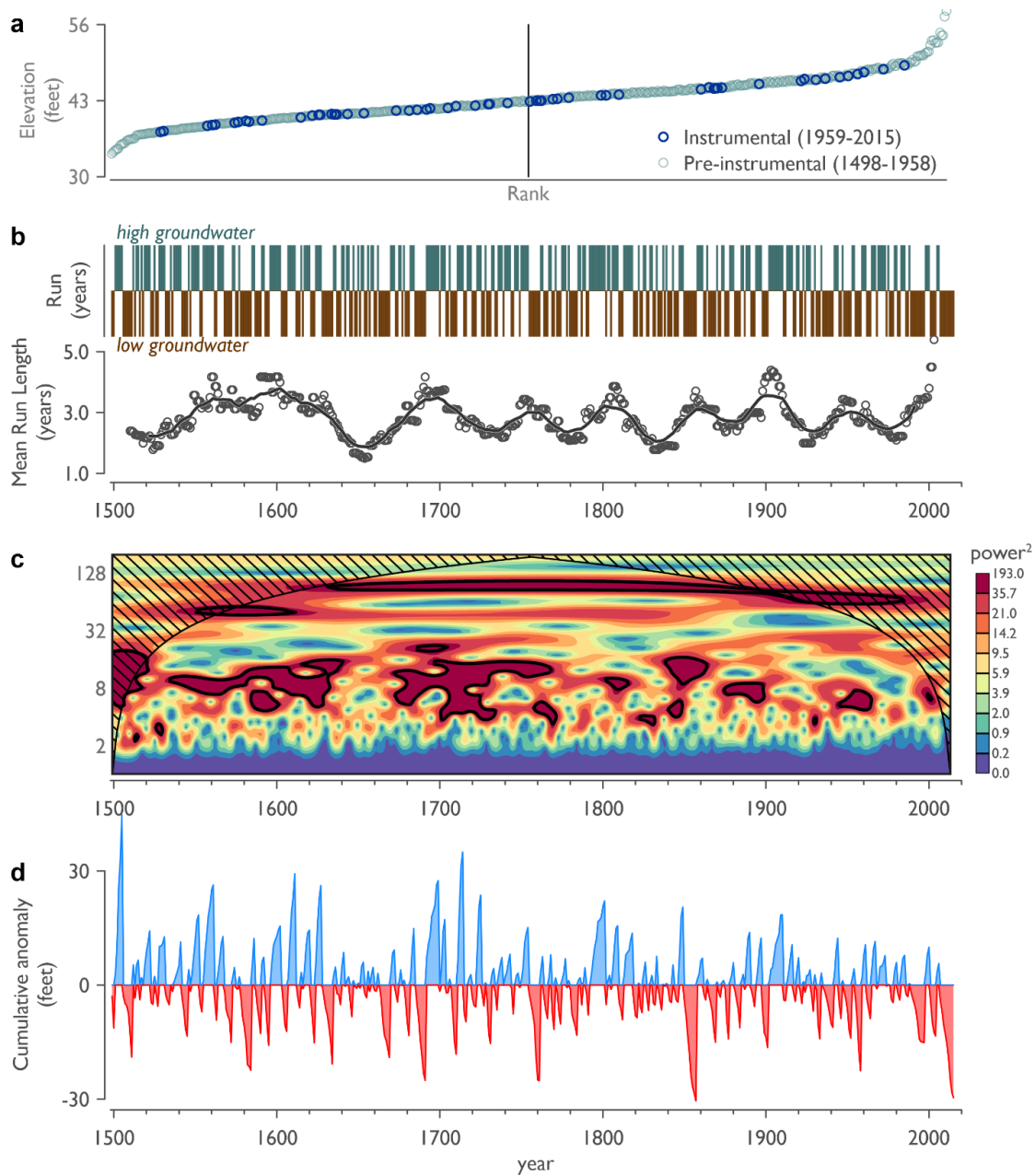
582 contributed to recent declines in groundwater elevation across the southeastern United States  
 583 (Vines et al., 2021), the potential amplification of these declines by groundwater extraction likely  
 584 resulted in the some of the lowest groundwater elevations in at least the past 500 years (Figure  
 585 4c, 7d).

586

587 **Table 2.** Years of extreme reconstructed groundwater elevations

Years of extreme low groundwater				Years of extreme high groundwater			
Reconstructed		Observed		Reconstructed		Observed	
year	Elevation (ft)	year	Elevation (ft)	year	Elevation (ft)	year	Elevation (ft)
1932	34.0	2002	35.4	1503	58.3	1965	52.4
1730	34.3	2012	36.5	1712	57.4	1966	51.2
1759	34.5	2001	36.8	1724	54.2	1960	49.3
1500	34.8	2011	37.3	1713	54.1	1998	48.5
1876	34.8	2008	37.9	1505	54.6	1970	48.1
1957	35.4	2009	38.7	1702	52.9	2019	48.0
1769	35.6	2010	39.0	1848	52.9	1961	47.8
1715	35.6	2007	39.0	1723	52.9	1984	47.7
1709	35.8	2003	39.3	1528	53.3	1959	47.2
1708	36.2	2013	39.3	1625	53.2	1967	47.2
1898	36.3	2000	39.4	1608	52.5	1987	46.8
1745	36.4	1963	40.0	1847	51.4	1983	46.3
1594	36.5	1981	40.1	1609	51.3	2018	45.9
1582	36.5	1990	40.1	1683	51.1	1988	45.6
1781	36.5	1977	40.2	1833	50.7	1986	45.5

588



589

590 **Figure 7.** Analysis of reconstructed groundwater elevation. (a) A ranked distribution of  
 591 groundwater elevation depicting the reconstructed values during the instrumental period relative  
 592 to the entire reconstruction. (b) Runs of consecutive years above- or below-average groundwater  
 593 elevations relative to the mean of the full reconstruction (1498–2015) shown as unique events  
 594 (top) and as a moving 25-yr average of the length of each run, regardless of the associated sign,  
 595 fit with a 25-year moving average for illustration purposes. (c) Wavelet power spectra of the

596 spliced groundwater reconstruction for North Central Florida. Black contours indicate significant  
597 power ( $p < 0.05$ ). Cross-hatched regions are the cone of influence where spectra may be distorted  
598 due to edge effects. (d) Cumulative anomalies shown as the sum of consecutive anomalies in  
599 each run of above- or below-average groundwater elevations.

600

601

602 2.6 Considering the influences of oceanic-atmospheric phenomena on groundwater

603 In Florida, multiple oceanic-atmospheric phenomena interact to influence patterns of  
604 atmospheric circulation that, in turn, drive hydrological variability and groundwater conditions.

605 These include the El Niño-Southern Oscillation (ENSO) and the Atlantic Multidecadal

606 Oscillation (AMO), both of which may be modulated through interactions with sea surface

607 temperatures in the north Pacific (Enfield et al., 2001; McCabe et al., 2008; McCabe et al., 2004;

608 Tootle & Piechota, 2006). Although the impacts of these phenomena are documented over the

609 instrumental record, their influence on the climate of northern Florida is variable over time,

610 particularly with respect to ENSO (Cole & Cook, 1998; Torbenson et al., 2019). The significant

611 band of 5–15 year periodicity identified through much of the reconstruction encapsulates ENSO-

612 scale forcing (Cane, 1986), as well as longer-term variability, while the 100-yr periodicity

613 identified in the reconstruction surpasses the canonical description of AMO variability (Enfield

614 et al., 2001; Newman et al., 2016). It is noteworthy that neither of these modes of variability in

615 the reconstruction precisely fit the observed scale at which these coupled oceanic-atmospheric

616 phenomena operate, and yet consistent patterns of increasing and decreasing persistence exist in

617 the reconstruction that reflect the oscillatory behavior associated with these processes. This

618 suggests the existence of inter-basin interactions of oceanic-atmospheric processes that drive the

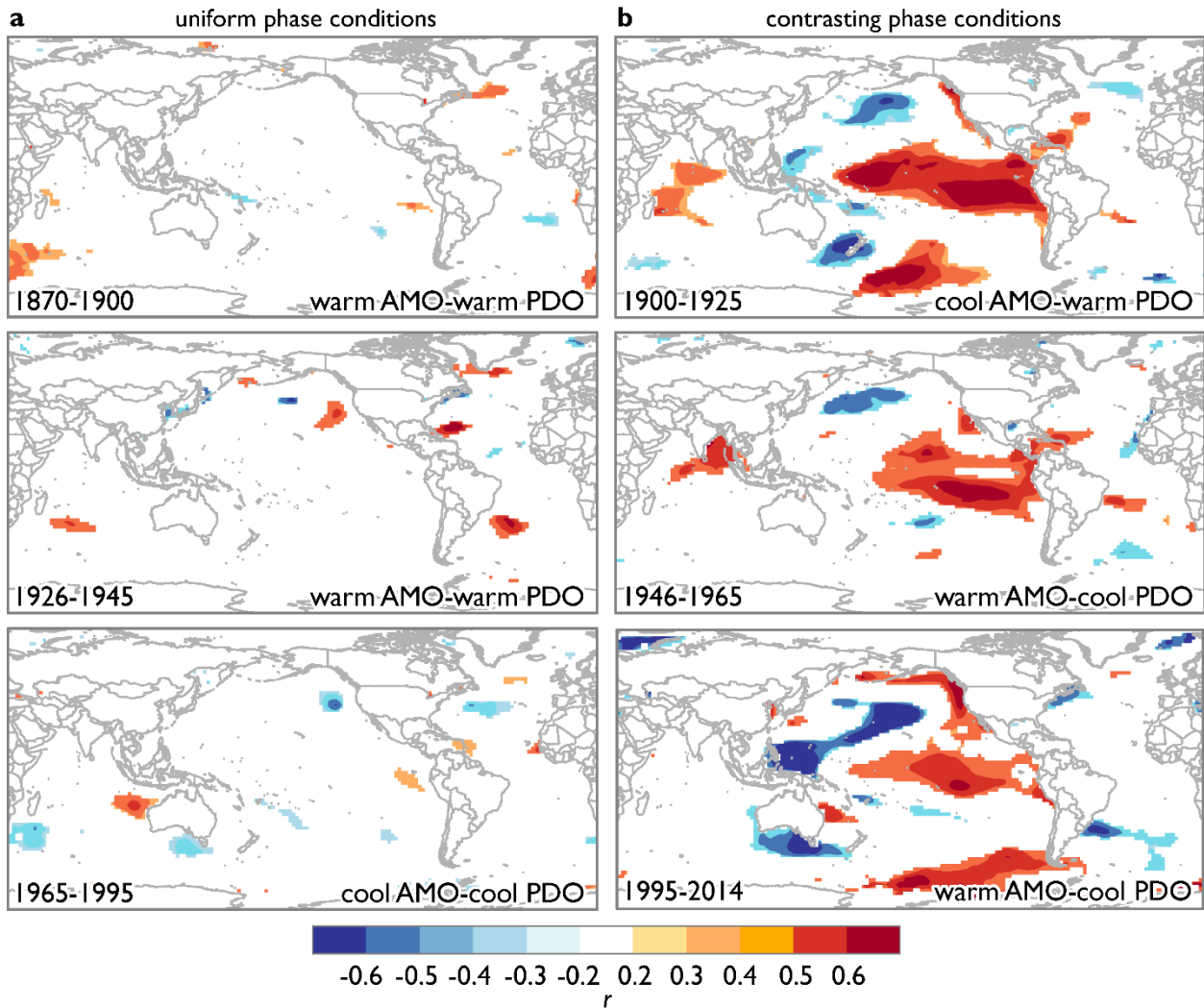
619 periodicity and variable persistence in groundwater elevations at our site. This is illustrated by  
620 examining the relationship between the reconstruction and global sea surface temperatures over  
621 time.

622

623 Correlations between the groundwater reconstruction and global SST (NCDC ERSST v5, Huang  
624 et al., 2017), calculated and visualized using KNMI Climate Explorer (Trouet & Van  
625 Oldenborgh, 2013), illustrate modulation of ENSO influences over time by contingent phases of  
626 the AMO and PDO (Dong et al., 2006; Li et al., 2013; Yeh & Kirtman, 2005). The influence of  
627 ENSO on groundwater elevation was strongest during periods of contrasting AMO and PDO  
628 phases and diminished during periods of coherent phases of these coupled oceanic-atmospheric  
629 phenomena (Figure 8). The temporal scope of this analysis was extended beyond the period of  
630 instrumental sea surface temperature records by comparing the groundwater elevation  
631 reconstruction to a suite of proxy-based reconstructions of ENSO variability that were variously  
632 based on tree-ring and coral records (Datwyler et al., 2019; Freund et al., 2019; Li et al., 2013;  
633 D. W. Stahle et al., 1998; Torbenson et al., 2019). Moving correlations over 25-year windows  
634 indicated widely varying relationships between groundwater elevation and each representation of  
635 ENSO activity (Figure 9). Taken together, these results underscore that northern Florida is within  
636 a region of intersection among multiple climate driver impacts (Maleski & Martinez, 2018), and  
637 that while this produces inconsistent patterns of teleconnection influences through time, the  
638 longer-term perspective of groundwater elevations enabled through this tree-ring-based  
639 reconstruction helps identify patterns in groundwater conditions that may prove helpful for  
640 groundwater resource projects. Specifically, understanding how the sea surface temperatures  
641 associated with contrasting phases of the AMO and PDO influence atmospheric circulation to

642 amplify ENSO influences on groundwater resources in northern Florida could enable forecasting  
 643 persistence and the likelihood of long-term water abundance or scarcity.

644

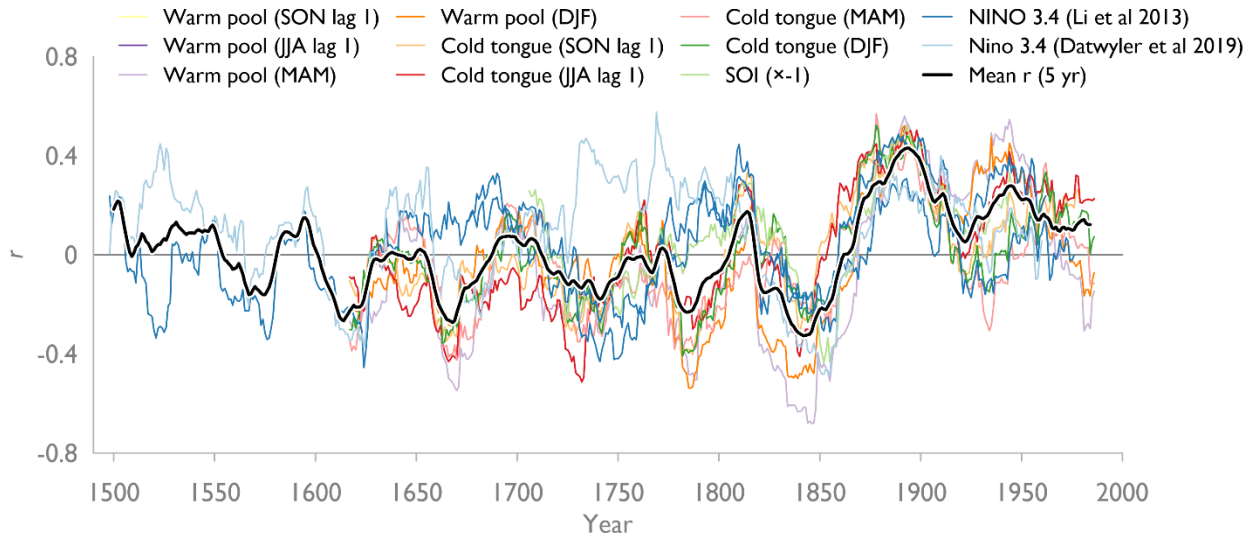


645

646

647 **Figure 8.** Shifting relationships between sea surface temperatures (SST) and reconstructed  
 648 groundwater elevation in North Central Florida. Correlations between annual groundwater  
 649 elevation and December–March NCDCE ERSST v5 sea surface temperatures during (a) periods of  
 650 similar AMO and PDO phases and (b) periods of contrasting AMO and PDO phases illustrate a  
 651 temporally variable influence of ENSO on North Central Florida hydrologic conditions.

652



653

654 **Figure 9.** Relationship between reconstructed North Central Florida groundwater and a suite of

655 proxy-based reconstructions of different aspects of El Niño-Southern Oscillation variability.

656 Values are the Pearson product moment correlation coefficient for the first year of moving 30-

657 year windows.

658

659

### 660 3. Conclusions

661 The reconstruction we report here expands tenfold the temporal perspective on groundwater

662 variability in North Central Florida. In doing so, we identified a high likelihood of recent low

663 groundwater elevations that reached levels comparable to past megadrought periods and suggest

664 that groundwater extraction likely magnified the influence of climate to drive these extreme

665 lows. Collectively, our results illustrate the cross-scale interactions of inter-basin oceanic-

666 atmospheric teleconnections that modulate the influence of ENSO variability on northern Florida

667 hydroclimate variability. These climate drivers create periods of greater and less persistence

668 within groundwater elevations that in turn produce prolonged periods of near-average conditions  
669 when persistence is low and pluvial or deep drought when persistence is high. Based on the past  
670 500 years of groundwater elevations, it appears that persistence is currently increasing and will  
671 likely do so for at least another decade. This suggests that water resource managers would do  
672 well to plan for sustained conditions that could continue current droughts or cause a switch to a  
673 prolonged pluvial. The amplification of future drought conditions by groundwater extraction will  
674 lead to water scarcity at levels not observed during the instrumental period.

675

## 676 **Acknowledgments**

677 Thanks go to Nick Flinner for his steadfast work developing initial tree-ring chronologies from  
678 old longleaf pine stumps, Zach Holmboe and Sam Horsnell for their assistance in the field, Fay  
679 Baird for help in the field and gathering and collating groundwater well data, and Mark Larson  
680 for his assistance in identifying sampling areas and understanding the history of Goethe State  
681 Forest. Neil Pederson provided insightful comments on an earlier version of this manuscript that  
682 helped refine our approach to reconstructing groundwater variability. Funding for this research  
683 was provided by the Suwannee River Water Management District. The authors declare no real or  
684 perceived conflicts of interest.

685

## 686 **Open Research**

687 Upon acceptance for publication, all tree-ring data developed for this study will be made publicly  
688 accessible through the International Tree-Ring Data Bank [available:  
689 <https://www.ncei.noaa.gov/products/paleoclimatology/tree-ring>], with the following statement  
690 then relevant:

691  
692 The tree-ring data used in the groundwater reconstruction are available at the International Tree-  
693 Ring Data Bank (<https://www.ncei.noaa.gov/products/paleoclimatology/tree-ring>) via [link;  
694 Goethe State Forest longleaf pine chronologies], [link2; Bald cypress chronologies], and [link3;  
695 Bald cypress chronologies]. Instrumental groundwater data used are available through the My  
696 Suwannee River Water Management District portal  
697 (<https://www.mysuwanneeriver.com/108/Groundwater-Levels>) via  
698 [[http://www.mysuwanneeriver.org/data/GWData/S101722001/S101722001\\_Level.xlsx](http://www.mysuwanneeriver.org/data/GWData/S101722001/S101722001_Level.xlsx);  
699 Newberry] and  
700 [[http://www.mysuwanneeriver.org/data/GWData/S101210001/S101210001\\_Level.xlsx](http://www.mysuwanneeriver.org/data/GWData/S101210001/S101210001_Level.xlsx); Cross  
701 City]. Figures were created using Grapher v15 software (<https://www.goldensoftware.com>) and  
702 maps were created in ArcGIS Pro v2.4 (<https://www.esri.com>).

703

704

## 705 **References**

706 Barlow, P. M. (2003). *Ground Water in Freshwater-Saltwater Environments of the Atlantic Coast.*

707 Reston, Virginia: U.S. Geological Survey Circular 1262.

708 BEBR. (2011). *Florida estimates of population 2010*. Retrieved from University of Florida Bureau

709 of Economic and Business Research, Gainesville, Florida:

710 [https://www.bibr.ufl.edu/population\\_repo\\_cats/florida-population-estimates/](https://www.bibr.ufl.edu/population_repo_cats/florida-population-estimates/)

711 BEBR. (2020). *Florida estimates of population 2020*. Retrieved from University of Florida Bureau

712 of Economic and Business Research, Gainesville, Florida:

713 [https://www.bibr.ufl.edu/population\\_repo\\_cats/florida-population-estimates/](https://www.bibr.ufl.edu/population_repo_cats/florida-population-estimates/)

- 714 Bierkens, M. F. P., & Wada, Y. (2019). Non-renewable groundwater use and groundwater  
715 depletion: a review. *Environmental Research Letters*, *14*(6), 063002.  
716 <https://doi.org/10.1088/1748-9326/ab1a5f>
- 717 Bunn, A. G. (2008). A dendrochronology program library in R (dplR). *Dendrochronologia*, *26*,  
718 115–124. <https://doi.org/10.1016/j.dendro.2008.01.002>
- 719 Buras, A. (2017). A comment on the expressed population signal. *Dendrochronologia*, *44*, 130–  
720 132. <https://doi.org/10.1016/j.dendro.2017.03.005>
- 721 Cane, M. A. (1986). El Niño. *Annual Review of Earth and Planetary Sciences*, *14*, 43–70.  
722 <https://doi.org/10.1146/annurev.ea.14.050186.000355>
- 723 Carr, D., & Stahle, D. W. (2010). *NOAA/WDS Paleoclimatology - Carr - Middle Withlacoochee*  
724 *River - TADI - ITRDB FL008*. NOAA National Centers for Environmental Information.  
725 <https://doi.org/10.25921/gqph-x765>. Accessed June 15, 2019.
- 726 Ciruzzi, D. M., & Loheide, S. P. (2021). Groundwater subsidizes tree growth and transpiration in  
727 sandy humid forests. *Ecohydrology*, *14*(5). <https://doi.org/10.1002/eco.2294>
- 728 Cole, J. E., & Cook, E. R. (1998). The changing relationship between ENSO variability and  
729 moisture balance in the continental United States. *Geophysical Research Letters*, *25*(24),  
730 4529–4532. <https://doi.org/10.1029/1998GL900145>
- 731 Cook, E. R. (1985). *A Time Series Analysis Approach to Tree Ring Standardization*. (Ph.D. Ph.D.  
732 Dissertation), University of Arizona, Tucson, Arizona.
- 733 Cook, E. R., & Krusic, P. J. (2013). ARSTAN v44h2: A tree-ring standardization program based  
734 on detrending and autoregressive time series modeling, with interactive graphics.  
735 Palisades, New York, USA: Tree-Ring Laboratory, Lamont-Doherty Earth Observatory of  
736 Columbia University.

- 737 Cook, E. R., & Peters, K. (1981). The smoothing spline: a new approach to standardizing forest  
738 interior tree-ring width series for dendroclimatic studies. *Tree-Ring Bulletin*, 41, 45–53.  
739 <http://hdl.handle.net/10150/261038>
- 740 Cook, E. R., & Peters, K. (1997). Calculating unbiased tree-ring indices for the study of climatic  
741 and environmental change. *The Holocene*, 7(3), 361–370.  
742 <https://doi.org/10.1177/095968369700700314>
- 743 Crockett, K., Martin, J. B., Grissino-Mayer, H. D., Larson, E. R., & Mirti, T. (2010). Assessment  
744 of tree rings as a hydrologic record in a humid subtropical environment. *Journal of the*  
745 *American Water Resources Association*, 46(5), 919–931. [https://doi.org/10.1111/j.1752-](https://doi.org/10.1111/j.1752-1688.2010.00464.x)  
746 [1688.2010.00464.x](https://doi.org/10.1111/j.1752-1688.2010.00464.x)
- 747 Datwyler, C., Abram, N. J., Grosjean, M., Wahl, E. R., & Neukom, R. (2019). El Nino-Southern  
748 Oscillation variability, teleconnection changes and responses to large volcanic eruptions  
749 since AD 1000. *International Journal of Climatology*, 39(5), 2711–2724. Article.  
750 <https://doi.org/10.1002/joc.5983>
- 751 de Graaf, I. E. M., Gleeson, T., van Beek, L. P. H., Sutanudjaja, E. H., & Bierkens, M. F. P. (2019).  
752 Environmental flow limits to global groundwater pumping. *Nature*, 574(7776), 90–94.  
753 <http://dx.doi.org/10.1038/s41586-019-1594-4>
- 754 Dong, B. W., Sutton, R. T., & Scaife, A. A. (2006). Multidecadal modulation of El Niño-Southern  
755 Oscillation (ENSO) variance by Atlantic Ocean sea surface temperatures. *Geophysical*  
756 *Research Letters*, 33(8), L08705. Article. <https://doi.org/10.1029/2006gl025766>
- 757 Enfield, D. B., Mestas-Nunez, A. M., & Trimble, P. J. (2001). The Atlantic multidecadal  
758 oscillation and its relation to rainfall and river flows in the continental US. *Geophysical*  
759 *Research Letters*, 28(10), 2077–2080. <https://doi.org/10.1029/2000GL012745>

- 760 Ferguson, G., & St. George, S. (2003). Historical and estimated ground water levels near  
761 Winnipeg, Canada, and their sensitivity to climatic variability. *Journal of the American*  
762 *Water Resources Association*, 39(5), 1249–1259. Article. [https://doi.org/10.1111/j.1752-](https://doi.org/10.1111/j.1752-1688.2003.tb03706.x)  
763 [1688.2003.tb03706.x](https://doi.org/10.1111/j.1752-1688.2003.tb03706.x)
- 764 Foster, T. E., & Brooks, J. R. (2001). Long-term trends in growth of *Pinus palustris* and *Pinus*  
765 *elliottii* along a hydrological gradient in central Florida. *Canadian Journal of Forest*  
766 *Research*, 31(10), 1661–1670. <https://doi.org/10.1139/x01-100>
- 767 Freund, M. B., Henley, B. J., Karoly, D. J., McGregor, H. V., Abram, N. J., & Dommenges, D.  
768 (2019). Higher frequency of Central Pacific El Niño events in recent decades relative to  
769 past centuries. *Nature Geoscience*, 12(6), 450–455. Article.  
770 <https://doi.org/10.1038/s41561-019-0353-3>
- 771 Fritts, H. C. (1976). *Tree Rings and Climate*. New York: Academic Press.
- 772 Gholami, V., Torkaman, J., & Khaleghi, M. R. (2017). Dendrohydrogeology in  
773 paleohydrogeologic studies. *Advances in Water Resources*, 110, 19–28. Article.  
774 <https://doi.org/10.1016/j.advwatres.2017.10.004>
- 775 Gordu, F., & Nachabe, M. H. (2021). Hindcasting multidecadal predevelopment groundwater  
776 levels in the Floridan aquifer. *Groundwater*, 59(4), 524–536. Article.  
777 <https://doi.org/10.1111/gwat.13073>
- 778 Griffin, D., Meko, D. M., Touchan, R., Leavitt, S. W., & Woodhouse, C. A. (2011). Latewood  
779 chronology development for summer-moisture reconstruction in the US Southwest. *Tree-*  
780 *Ring Research*, 67(2), 87–101. <https://doi.org/10.3959/2011-4.1>
- 781 Harley, G. L., Maxwell, J. T., Larson, E., Grissino-Mayer, H. D., Henderson, J., & Huffman, J.  
782 (2017). Suwannee River flow variability 1550–2005 CE reconstructed from a multispecies

- 783 tree-ring network. *Journal of Hydrology*, 544, 438–451.  
784 <http://dx.doi.org/10.1016/j.jhydrol.2016.11.020>
- 785 Huang, B., Thorne, P. W., Banzon, V. F., Boyer, T., Chepurin, G., Lawrimore, J. H., et al. (2017).  
786 Extended reconstructed sea surface temperature, version 5 (ERSSTv5): Upgrades,  
787 validations, and intercomparisons. *Journal of Climate*, 30(20), 8179–8205.  
788 <https://doi.org/10.1175/jcli-d-16-0836.1>
- 789 Huffman, J. M., & Rother, M. T. (2017). Dendrochronological field methods for fire history in  
790 pine ecosystems of the Southeastern Coastal Plain. *Tree-Ring Research*, 73(1), 42–46.  
791 <https://doi.org/10.3959/1536-1098-73.1.42>
- 792 Hunter, S. C., Allen, D. M., & Kohfeld, K. E. (2020). Comparing approaches for reconstructing  
793 groundwater levels in the mountainous regions of interior British Columbia, Canada, using  
794 tree ring widths. *Atmosphere*, 11(12), 25. Article. <https://doi.org/10.3390/atmos11121374>
- 795 Jasechko, S., & Perrone, D. (2021). Global groundwater wells at risk of running dry. *Science*,  
796 372(6540), 418-+. Article. <https://doi.org/10.1126/science.abc2755>
- 797 Li, J. B., Xie, S. P., Cook, E. R., Morales, M. S., Christie, D. A., Johnson, N. C., et al. (2013). El  
798 Niño modulations over the past seven centuries. *Nature Climate Change*, 3(9), 822–826.  
799 Article. <https://doi.org/10.1038/nclimate1936>
- 800 Maleski, J. J., & Martinez, C. J. (2018). Coupled impacts of ENSO AMO and PDO on temperature  
801 and precipitation in the Alabama–Coosa–Tallapoosa and Apalachicola–Chattahoochee–  
802 Flint river basins. *International Journal of Climatology*, 38(S1), e717–e728.  
803 <https://doi.org/10.1002/joc.5401>

- 804 Marella, R. L., & Berndt, M. P. (2005). *Water withdrawals and trends from the Floridan aquifer*  
805 *system in the southeastern United States, 1950-2000*. Reston, Virginia: U.S. Geological  
806 Survey Circular 1278.
- 807 McCabe, G. J., Betancourt, J. L., Gray, S. T., Palecki, M. A., & Hidalgo, H. G. (2008).  
808 Associations of multi-decadal sea-surface temperature variability with US drought.  
809 *Quaternary International*, 188, 31–40. Proceedings Paper.  
810 <https://doi.org/10.1016/j.quaint.2007.07.001>
- 811 McCabe, G. J., Palecki, M. A., & Betancourt, J. L. (2004). Pacific and Atlantic Ocean influences  
812 on multidecadal drought frequency in the United States. *Proceedings of the National*  
813 *Academy of Sciences of the United States of America*, 101(12), 4136–4141.  
814 <https://doi.org/10.1073/pnas.0306738101>
- 815 McCarroll, D., Young, G. H., & Loader, N. J. (2015). Measuring the skill of variance-scaled  
816 climate reconstructions and a test for the capture of extremes. *The Holocene*, 25(4), 618–  
817 626. <https://doi.org/10.1177/0959683614565956>
- 818 Meko, D. M. (1981). *Application of Box-Jenkins methods of time series analysis to the*  
819 *reconstruction of drought from tree rings*. (Ph.D. Ph.D. Dissertation), University of  
820 Arizona, Tucson, Arizona.
- 821 Miller, J. A. (1990). *Ground Water Atlas of the United States: Segment 6, Alabama, Florida,*  
822 *Georgia, South Carolina* (730G). Retrieved from  
823 <http://pubs.er.usgs.gov/publication/ha730G>
- 824 NCDC. (2018). Monthly Historical Climate Time Series. Retrieved from  
825 <https://www7.ncdc.noaa.gov/CDO/CDODivisionalSelect.jsp>

- 826 Newman, M., Alexander, M. A., Ault, T. R., Cobb, K. M., Deser, C., Lorenzo, E. D., et al. (2016).  
827 The Pacific Decadal Oscillation, revisited. *Journal of Climate*, 29(12), 4399–4427.  
828 <https://doi.org/10.1175/JCLI-D-15-0508.1>
- 829 Outland III, R. B. (2004). *Tapping the Pines: The Naval Stores Industry in the American South*.  
830 Baton Rouge, Louisiana: LSU Press.
- 831 Pederson, N., Bell, A. R., Knight, T. A., Leland, C., Malcomb, N., Anchukaitis, K. J., et al. (2012).  
832 A long-term perspective on a modern drought in the American Southeast. *Environmental*  
833 *Research Letters*, 7(1), 014034. <https://doi.org/10.1088/1748-9326/7/1/014034>
- 834 Perez-Valdivia, C., & Sauchyn, D. (2011). Tree-ring reconstruction of groundwater levels in  
835 Alberta, Canada: Long term hydroclimatic variability. *Dendrochronologia*, 29(1), 41–47.  
836 <http://dx.doi.org/10.1016/j.dendro.2010.09.001>
- 837 R Development Core Team. (2019). R: A language and environment for statistical computing  
838 (Version v2.11.1). Vienna, Austria: R Foundation for Statistical Computing. Retrieved  
839 from <http://www.R-project.org>
- 840 Schmidt, N., Lipp, E. K., Rose, J. B., & Luther, M. E. (2001). ENSO influences on seasonal rainfall  
841 and river discharge in Florida. *Journal of Climate*, 14(4), 615–628.  
842 [https://doi.org/10.1175/1520-0442\(2001\)014<0615:EIOSRA>2.0.CO;2](https://doi.org/10.1175/1520-0442(2001)014<0615:EIOSRA>2.0.CO;2)
- 843 SRWMD. (2020). Suwannee River Water Management District Groundwater Portal.
- 844 Stahle, D. W., Carr, D., Griffin, R. D., & Jennings, J. (2010). *NOAA/WDS Paleoclimatology -*  
845 *Stahle - Upper Withlacoochee River - TADI - ITRDB FL009*. NOAA National Centers for  
846 Environmental Information. <https://doi.org/10.25921/gqph-x765>. Accessed June 15, 2019.
- 847 Stahle, D. W., D'Arrigo, R., Krusic, P. J., Cleaveland, M. K., Cook, E., Allan, R. J., et al. (1998).  
848 Experimental dendroclimatic reconstruction of the Southern Oscillation. *Bulletin of the*

- 849 *American Meteorological Society*, 79(10), 2137–2152. [https://doi.org/10.1175/1520-](https://doi.org/10.1175/1520-0477(1998)079<2137:EDROTS>2.0.CO;2)  
850 [0477\(1998\)079<2137:EDROTS>2.0.CO;2](https://doi.org/10.1175/1520-0477(1998)079<2137:EDROTS>2.0.CO;2)
- 851 Stahle, D. W., Fye, F. K., Cook, E. R., & Griffin, R. D. (2007). Tree-ring reconstructed  
852 megadroughts over North America since A.D. 1300. *Climatic Change*, 83(1), 133–149.  
853 journal article. <https://doi.org/10.1007/s10584-006-9171-x>
- 854 Sutton, C., Kumar, S., Lee, M. K., & Davis, E. (2021). Human imprint of water withdrawals in the  
855 wet environment: A case study of declining groundwater in Georgia, USA. *Journal of*  
856 *Hydrology-Regional Studies*, 35, 16. Article. <https://doi.org/10.1016/j.ejrh.2021.100813>
- 857 Tegel, W., Seim, A., Skiadaresis, G., Ljungqvist, F., Kahle, H.-P., & Land, A. (2020). Higher  
858 groundwater levels in western Europe characterize warm periods in the Common Era.  
859 *Scientific Reports*, 10. <https://doi.org/10.1038/s41598-020-73383-8>
- 860 Tootle, G. A., & Piechota, T. C. (2006). Relationships between Pacific and Atlantic ocean sea  
861 surface temperatures and U.S. streamflow variability. *Water Resources Research*, 42(7),  
862 W07411. <https://doi.org/10.1029/2005wr004184>
- 863 Torbenson, M. C. A., Stahle, D. W., Howard, I. M., Burnette, D. J., Villanueva-Diaz, J., Cook, E.  
864 R., & Griffin, D. (2019). Multidecadal modulation of the ENSO teleconnection to  
865 precipitation and tree growth over subtropical North America. *Paleoceanography and*  
866 *Paleoclimatology*, 34(5), 886–900. Article. <https://doi.org/10.1029/2018pa003510>
- 867 Torrence, C., & Compo, G. P. (1998). A practical guide to wavelet analysis. *Bulletin of the*  
868 *American Meteorological Society*, 79(1), 61–78. [https://doi.org/10.1175/1520-](https://doi.org/10.1175/1520-0477(1998)079<0061:APGTWA>2.0.CO;2)  
869 [0477\(1998\)079<0061:APGTWA>2.0.CO;2](https://doi.org/10.1175/1520-0477(1998)079<0061:APGTWA>2.0.CO;2)

- 870 Trouet, V., & Van Oldenborgh, G. J. (2013). KNMI Climate Explorer: A web-based research tool  
871 for high-resolution paleoclimatology. *Tree-Ring Research*, 69(1), 3–13.  
872 <https://doi.org/10.3959/1536-1098-69.1.3>
- 873 Vines, M., Tootle, G., Terry, L., Elliott, E., Corbin, J., Harley, G. L., et al. (2021). A paleo  
874 perspective of Alabama and Florida (USA) interstate streamflow. *Water*, 13(5), 657–668.  
875 <https://doi.org/10.3390/w13050657>
- 876 Volk, M. I., Hctor, T. S., Nettles, B. B., Hilsenbeck, R., Putz, F. E., & Oetting, J. (2017). Florida  
877 Land Use and Land Cover Change in the Past 100 Years. In E. P. Chassignet, J. W. Jones,  
878 V. Misra, & J. Obeysekera (Eds.), *Florida's climate: Changes, variations, & impacts* (pp.  
879 51–82). Gainesville, Florida: Florida Climate Institute.
- 880 Wigley, T. M. L., Briffa, K. R., & Jones, P. D. (1984). On the average value of correlated time  
881 series, with applications in dendroclimatology and hydrometeorology. *Journal of Climate*  
882 *and Applied Meteorology*, 23(2), 201–213. [https://doi.org/10.1175/1520-](https://doi.org/10.1175/1520-0450(1984)023<0201:OTAVOC>2.0.CO;2)  
883 [0450\(1984\)023<0201:OTAVOC>2.0.CO;2](https://doi.org/10.1175/1520-0450(1984)023<0201:OTAVOC>2.0.CO;2)
- 884 Wise, E. K., & Dannenberg, M. P. (2019). Climate factors leading to asymmetric extreme capture  
885 in the tree-ring record. *Geophysical Research Letters*, 46(6), 3408–3416.  
886 <https://doi.org/10.1029/2019gl082295>
- 887 Yeh, S. W., & Kirtman, B. P. (2005). Pacific decadal variability and decadal ENSO amplitude  
888 modulation. *Geophysical Research Letters*, 32(5). <https://doi.org/10.1029/2004GL021731>
- 889 Zang, C., & Biondi, F. (2015). treeclim: an R package for the numerical calibration of proxy-  
890 climate relationships. *Ecography*, 38(4), 431–436. <https://doi.org/10.1111/ecog.01335>